Microanalysis Techniques to Study Atmospheric Ice Nucleation and Ice Crystal Growth

Daniel A. Knopf[1]

[1]School of Marine and Atmospheric Sciences, Stony Brook University, Stony Brook NY 11794-5000, USA

Index terms

Aerosol and particles, cloud physics and chemistry, cloud/radiation interaction, Techniques applicable in three or more fields

Keywords

Aerosol, ice nucleation, ice crystal, ice-nucleating particle, microanalysis techniques, nucleation theory

Abstract

The prediction of how ice crystals form represents one of the great conundrums in the atmospheric sciences with important implications for the hydrological cycle and climate. Ice-nucleating particles (INPs), typically consisting of sub- and supermicrometer-sized aerosol particles which can be inorganic, organic, biogenic, or biological, initiate heterogeneous ice nucleation processes leading to ice crystal formation. Heterogeneous ice nucleation commences on the nanoscale at the substrate surface and depends on ambient temperature and humidity. Microanalysis techniques are uniquely suited to examine the physicochemical features of the INPs under relevant atmospheric conditions thereby advancing our understanding of the principal processes that promote ice nucleation. In the atmosphere ice crystals experience growth and sublimation resulting in complex microscopic morphologies which, in turn, impact the ice crystal's properties. This chapter provides an overview of microanalysis techniques employed in either a multimodal or in situ manner, which shed light on the atmospheric heterogeneous ice

nucleation process and how these techniques are applied to explore the complex morphologies of ice crystals. The first section introduces the various atmospheric ice nucleation pathways, provides a brief outline of the underlying nucleation theory demonstrating that nucleation proceeds on the nanoscale, and describes the different ice crystal habits of growth. Section two provides an overview of the microanalysis techniques and experiments to study INPs or ice-nucleating substrates including multimodal instrument approaches followed by in situ ice nucleation studies. Examples of techniques include Raman, atomic force, electron, and X-ray microscopy with discussion of the techniques' unique capabilities to examine the physical and chemical properties of the ice-nucleating substrate. The third section presents electron microscopy studies of ice crystals during growth and sublimation displaying the morphological complexities of ice crystals. Lastly, section four discusses typical experimental requirements including sample sizes, radiation effects, and the role of standard INPs.

1 Introduction

Understanding the formation of ice crystals from atmospheric aerosol particles is one of the grand challenges in the atmospheric sciences. How and which aerosol particles serve as ice-nucleating particles (INPs) is relevant for our understanding of the microphysical cloud structure that in turn impacts the hydrological cycle and climate [*Boucher et al.*, 2013]. In the atmosphere two cloud regimes exist that contain ice particles which include cirrus clouds that consist of only ice crystals, typically present at heights above 6 km and temperatures below the homogeneous freezing limit of water at ~235 K, and, at higher temperatures, mixed-phase clouds in which supercooled water droplets and ice crystals coexist [*Koop et al.*, 2000; *Murray et al.*, 2012; *Storelvmo*, 2017]. Most precipitation is initiated by the formation of ice crystals [*Lau and Wu*,

2003; *Lohmann and Feichter*, 2005; *Mülmenstädt et al.*, 2015]. Furthermore, the presence of the ice phase can modulate the water vapor budget, of importance since it is the strongest greenhouse gas [*Held and Soden*, 2000; *Lohmann et al.*, 1995]. Cloud ice impacts cloud lifetime and albedo, thereby modulating the cloud's interaction with incoming shortwave and outgoing longwave radiation, in so doing affecting the radiative balance and thus, climate [*Baker and Peter*, 2008; *Baker*, 1997; *Boucher et al.*, 2013; *Lohmann and Feichter*, 2005; *Rosenfeld et al.*, 2014; *Storelvmo*, 2017; *Storelvmo et al.*, 2011].

The reasons that make prediction of atmospheric ice crystal formation difficult are manifold. Several different ice formation paths exist, and each shows different dependencies on temperature (T), relative humidity (RH), and particle morphology [*Hoose and Möhler*, 2012; *Kanji et al.*, 2017; *Knopf et al.*, 2018; *Marcolli*, 2014; *Pruppacher and Klett*, 1997; *Vali et al.*, 2015]. Ice nucleation is considered a rare event where only a small fraction of the ambient aerosol particles, sometimes only one in 100000, act as an INP [*DeMott et al.*, 2010; *Kanji et al.*, 2017]. Lastly, the INPs can be multiphase and multicomponent in nature, thus, physicochemically complex, and include inorganic, organic, biogenic, and biological matter [*Cziczo et al.*, 2017; *Kanji et al.*, 2017; *Knopf et al.*, 2018; *Murray et al.*, 2012].

Homogeneous ice nucleation proceeds from water and aqueous solution droplets and is mostly of importance for cirrus cloud formation. In this chapter, the focus is on heterogeneous ice nucleation that is facilitated by a substrate, in this case the INP, and, thus, is a surface-specific process proceeding on the nanoscale. Any substrate that does not dissolve, due to water uptake, over time scales necessary to induce ice nucleation can serve as an INP. Under typical atmospheric thermodynamic conditions, i.e., T and supersaturation with respect to the ice phase (S_{ice}), as will be made clear below, the critical ice nucleus that initiates ice formation is typically

the size of a few nanometers. As such, the study of heterogeneous ice nucleation from substrates is a truly formidable and challenging topic for the application of various microanalysis techniques.

1.1 Ice nucleation pathways

In the atmosphere different ice formation pathways exist. This chapter focuses on primary ice formation where ice nucleation is initiated by INPs. Secondary ice processes (SIPs) are recognized to contribute to, and in instances possibly dominate, the ambient ice crystal number concentrations [*Field et al.*, 2017; *Korolev and Leisner*, 2020; *Zipori et al.*, 2018]. However, SIPs typically do not involve a substrate which facilitates the nucleation process but include, e.g., shattering during droplet freezing, rime splintering, and fragmentation upon collision [*Field et al.*, 2017; *Korolev and Leisner*, 2020].

Ice formation in the atmosphere proceeds by either homogeneous ice nucleation or heterogeneous ice nucleation. Figure 1 provides a schematic overview of the prevailing primary ice nucleation mechanisms [*Knopf et al.*, 2018]. Homogeneous ice nucleation involves liquid droplets composed of either pure water or aqueous solutions in absence of a substrate facilitating the nucleation process (Fig. 1A). Hence, homogeneous ice nucleation requires lower temperatures and higher S_{ice} compared to heterogeneous ice nucleation. Micrometer-sized pure water droplets freeze homogeneously at about 235 K that corresponds to $S_{ice} \approx 1.5$. Aqueous solution droplets will experience a freezing point depression and thus will freeze homogeneously at lower T and higher S_{ice} [*Koop et al.*, 2000]. Only the presence of INPs results in ice nucleation between the homogeneous freezing limit and the melting point of ice (273.15 K). Heterogeneous ice nucleation can also proceed below ~235 K, typically at S_{ice} values that are below the required S_{ice} for homogeneous ice nucleation of about 1.5 to 1.7 [*Koop et al.*, 2000].

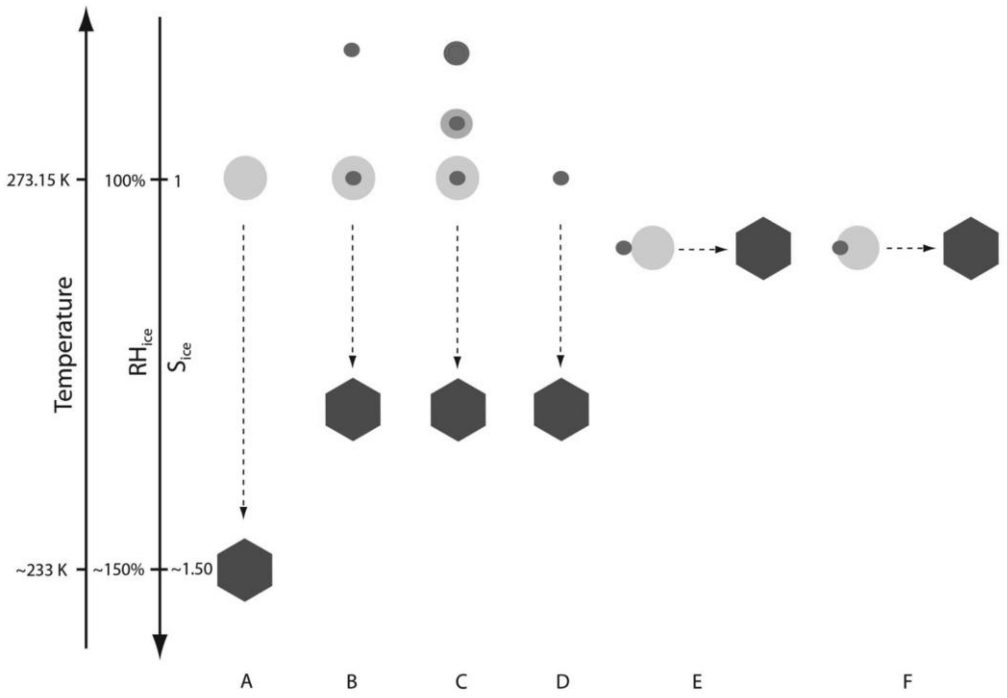

Figure 1. Representation of the various possible atmospheric ice nucleation pathways given for a range of temperature, relative humidity with respect to ice (RH_{ice}), and supersaturation with respect to ice (S_{ice}). Large circles and hexagons display liquid water and ice, respectively. Small dark circles represent the ice-nucleating particle (INP). In (C) INP is coated by an inorganic or organic coating and its aqueous solution. Ice formation pathways A to F represent homogeneous ice nucleation (A), immersion freezing (B), deliquescence and water uptake followed by immersion freezing (C), deposition ice nucleation (D), contact ice nucleation (E), and inside-out freezing (F). From *Knopf et al.* [2018].

Ice nucleation pathway (B) displays immersion freezing where the INP is immersed in supercooled water or aqueous solution droplets. Immersion freezing is recognized as the dominant primary ice formation pathway in mixed-phase cloud regimes [*Ansmann et al.*, 2009; *de Boer et al.*, 2011; *Westbrook and Illingworth*, 2013] where supercooled droplets and ice crystals can coexist. Pathway (C) represents water uptake and potential deliquescence of hygroscopic matter associated with the INP prior to immersion freezing. This can include amorphous organic compounds that continuously deliquesce upon increasing RH [*Berkemeier et al.*, 2014; *Knopf et al.*, 2018; *Koop et al.*, 2011; *Wang et al.*, 2012a] instead of showing a sharp solid-to-liquid transition as it is typical for salts [*Martin*, 2000]. If the condensation of liquid coincides with freezing within the supercooled temperature regime, the process is also termed

condensation freezing. Though on a microscopic level, it likely proceeds as immersion freezing [*Coluzza et al.*, 2017; *Wex et al.*, 2014]. Deposition ice nucleation is present in pathway (D), where ice forms on the INP from the supersaturated gas phase. Recently this concept has been questioned, with the suggestion that in the presence of nanopores, ice formation is initiated by pore condensation freezing [*David et al.*, 2019; *Marcolli*, 2014; 2020]. The underlying idea is based on water in nanopores having a large negative meniscus, thereby greatly reducing the water saturation pressure. This in turn, yields sufficiently high S_{ice} that allow for homogeneous ice nucleation to proceed in those pores. Deposition ice nucleation can contribute to ice crystal formation at lower temperatures and water subsaturated conditions representing cirrus cloud regimes, typical of the upper troposphere [*Cziczo et al.*, 2013; *DeMott*, 2002; *Heymsfield et al.*, 2017]. Pathway (E) displays contact ice nucleation where an INP collides with a supercooled droplet, thereby initiating freezing of the droplet [*Ladino Moreno et al.*, 2013]. Lastly, pathway (F) represents inside-out freezing where the INP in the supercooled temperature regime is in contact with the gas phase and aqueous phase as the droplet is evaporating [*Durant and Shaw*, 2005; *Shaw et al.*, 2005].

1.2 Ice nucleation kinetics

For a substrate to promote ice nucleation heterogeneously, classically the following requirements are assumed [*Hegg and Baker*, 2009; *Knopf et al.*, 2018; *Pruppacher and Klett*, 1997; *Vali et al.*, 2015]: (i) the substrate must be insoluble, (ii) it must be larger than the critical ice nucleus, (iii) its surface must have chemical bonds that can interact with and arrange water molecules, (iv) it must have a crystallographic match representing geometrical arrangement of bonds, or (v) there must be active sites of varying quality representing localized phenomena on the substrate surface. Following classical nucleation theory (CNT), for the formation of ice from supercooled

water a Gibbs free energy barrier has to be overcome to allow for the growth of a critical ice nucleus beyond the critical radius, r_{crit}. r_{crit} and the Gibbs free energy change, ΔG, can be derived as [*Alpert et al.*, 2011; *Pruppacher and Klett*, 1997; *Zobrist et al.*, 2007]:

$$r_{crit} = \frac{2\sigma_{sl}(T)\cdot v_s(T)}{kT \ln S(T)} \quad \text{and} \quad \Delta G(T) = \frac{16\pi\sigma_{sl}^3(T)\cdot v_s^2(T)}{3(kT \ln S_{ice}(T))^2}, \tag{1}$$

where σ_{sl} is the interfacial tension between ice (solid) and water (liquid), v_s is the volume of a water molecule in ice (solid), and k is the Boltzmann constant.

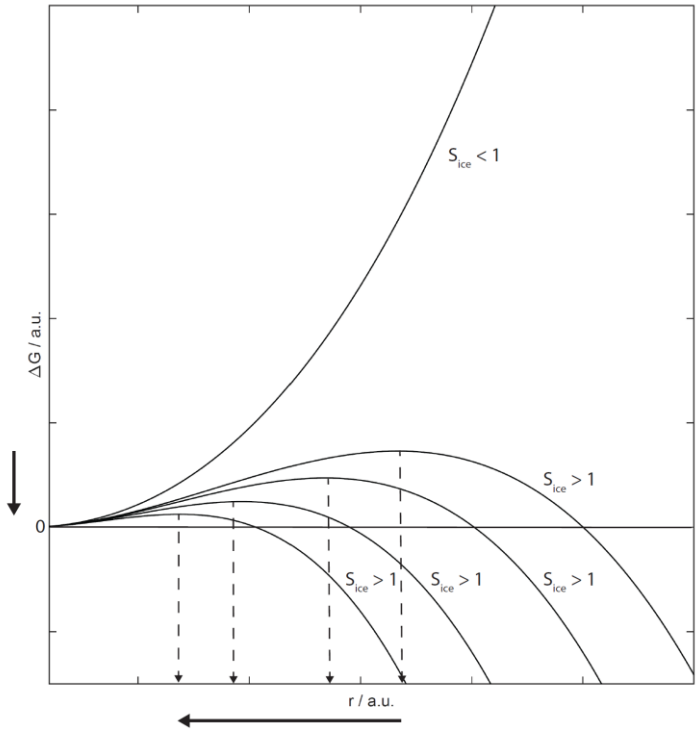

Figure 2. The change in Gibbs free energy necessary for the formation of a critical ice nucleus as a function of ice nucleus radius and supersaturation with respect to ice, S_{ice}. Solid black arrows indicate the decreasing Gibbs free energy barrier and decreasing radius with increasing S_{ice}. Dashed vertical arrows display how the critical radius decreases as S_{ice} increases.

Figure 2 outlines the behavior of the Gibbs free energy change with radius as a function of S_{ice}. For ice, subsaturated conditions (or above the ice melting temperature of 273.15 K) the activation barrier ΔG becomes infinite. As S_{ice} increases, ΔG and r_{crit} decrease as indicated by

the arrows in Fig. 2. Clearly, changes in S_{ice} determine the likelihood of establishing and maintaining the critical ice nucleus, so that nucleation and freezing commences.

Figure 3 displays the change of r_{crit} as a function of temperature for pure water in relation to typical particle surface areas. For typical conditions of atmospheric heterogeneous ice nucleation, the critical ice nucleus size has a radius of about 1 nm (Fig. 3a). This implies that surface features that enable ice nucleation are in the order of 1 to 20 nm^2 (Fig. 3b). A spherical

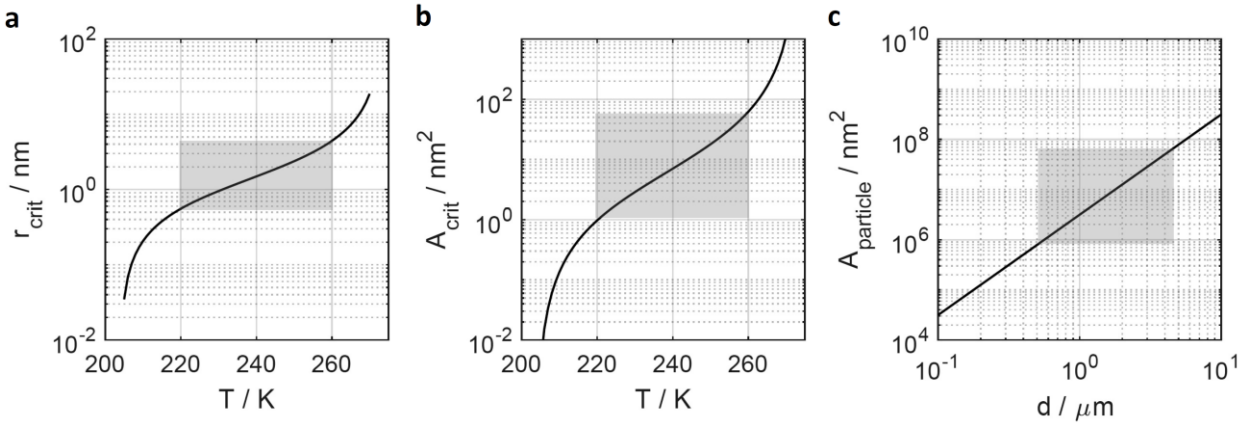

Figure 3. Estimates of (a) the critical ice nucleus radius (r_{crit}) and (b) its surface area (A_{crit}) as a function of temperature using Eq. (1). For comparison the surface area of spherical particles ($A_{particle}$) is given in (c). Shading in (a) and (b) indicates typical atmospheric conditions for heterogeneous ice nucleation. Shading in (c) indicates typical ice-nucleating particle sizes and surface areas.

particle of 1 µm in size has a surface area of about 3×10^6 nm^2, allowing for the presence of a large number of surface features that could initiate ice nucleation (Fig. 3c). Considering these large numbers of sites, it can be assumed that it is very likely that sufficient surface features representing the ice-nucleating surface material should always be present. Looking at these features on microscopic scales, application of microanalysis techniques are uniquely suited to advance our understanding of the ice nucleation process.

The heterogeneous ice nucleation rate coefficient, J_{het}, for immersion freezing is defined as the number of nucleation events per surface area and time, given in units cm^{-2} s^{-1}. It can be derived using $\Delta G(T)$ and a diffusion activation energy for a water molecule to cross the water –

ice nucleus interface, $\Delta F_{diff}(T)$ [*Alpert et al.*, 2011; *Pruppacher and Klett*, 1997; *Turnbull and Fisher*, 1949; *Zobrist et al.*, 2007]:

$$J_{het}(T) = \frac{kT}{h} e^{\left[-\frac{\Delta F_{diff}(T)}{kT}\right]} n e^{\left[-\frac{\Delta G(T) f_{het}(m,)}{kT}\right]}. \quad (2)$$

The pre-factor serves as an impinging frequency given by $\frac{kT}{h}$, where h is Planck's constant. n represents the number of water molecules at the INP-water interface and can be assumed to be around 10^{15} cm^{-2}. $\Delta F_{diff}(T)$ depends on the diffusivity of water that can be expressed by the Vogel-Fulcher-Tammann equation [*Smith and Kay*, 1999]. $f_{het}(m, x)$ is the so-called geometric factor, where m is the compatibility factor and x represents the ratio of the radius of the substrate to the radius of spherical critical ice nucleus [*Knopf et al.*, 2022]. x can be neglected when particles are larger than 0.1 μm. This holds for most INPs and thus, we can write $\lim_{x\to\infty} f_{het}(m, x) = \frac{m^3-3m+2}{4}$. Instead of reporting m, typically the contact angle, θ, is given. θ is derived from $\cos\theta = m$ [*Fletcher*, 1958]. A smaller θ value indicates a more efficient INP. The extreme case of an inefficient INP is represented by $\theta = 180°$ which indicates the case of homogeneous ice nucleation. In other words, for $f_{het}(m, x) = 1$, Eq. (2) represents the case of homogeneous ice nucleation from a supercooled liquid droplet.

For the derivation of the deposition ice nucleation rate coefficients [*Alpert et al.*, 2011; *Pruppacher and Klett*, 1997; *Wang and Knopf*, 2011], the diffusion activation energy is omitted, and n represents the number of water adsorption sites on the INP surface and can be assumed to be around 10^{15} cm^{-2}. σ_{sl} is exchanged for the interfacial tension between ice (solid) and supersaturated gas phase (vapor), σ_{sv}.

The above descriptive approaches for capturing the immersion freezing and deposition ice nucleation kinetics follow CNT [*Pruppacher and Klett*, 1997]. As such, the nucleation process is

considered to be stochastic and, thus, is implicitly time dependent, resulting in $J_{het}(T)$ [*Knopf et al.*, 2020]. This in turn leads to the question of how many ice nucleation events have to be observed to obtain statistical significance. Based on a binomial distribution for freezing probabilities, upper and lower fiducial limits for observed nucleation events at a given confidence level can be derived [*Koop et al.*, 1997]. For example, observation of a single ice nucleation event, leads to a maximum of 9.233 and minimum of 0.001 nucleation events at a confidence level of 0.999. *Alpert and Knopf* [2016] suggest observing at least 100-200 ice nucleation events to keep corresponding uncertainties in freezing kinetics within ±1 order of magnitude. The issue of statistical uncertainty can directly affect how to best observe particle or substrate samples using microanalysis techniques. The minimum required number of observed ice nucleation events can define the chosen sample size and field of view. If the focus is on the investigation of physicochemical surface properties that induce ice nucleation instead of nucleation kinetics, the total number of observed ice nucleation events may not be as important, though one should examine several independent samples to ensure reproducibility.

A common approach for characterizing and comparing ice nucleation efficacies of INPs is the ice nucleation active site (INAS) description [*Connolly et al.*, 2009; *Vali*, 1971]. This approach is based on the deterministic or singular hypothesis method. It ignores the stochastic nature of nucleation and, thus, is time independent. In this case, nucleation efficacies are expressed as INAS densities, $n_s(T)$, in units cm^{-2}, providing the number of ice nucleation events per surface area at a given temperature. This description implies that each ice nucleation event is associated with a characteristic INAS.

The concept of what establishes an INAS is a current matter of research. Characterization of an INAS requires greater resolution than is required to determine the size of the critical ice

nucleus (Fig. 3) and has yet not been achieved in situ. This is the case if the arrangement of a critical ice nucleus proceeds only at one site. However, one can envision that several ice-like clusters emerge across the given surface area that could subsequently combine to form a larger critical ice nucleus, thus, surpassing r_{crit}. Clearly, the minute scale of an active site poses a challenge even for the most advanced microanalysis techniques. Application of alternative computational approaches, like molecular dynamics simulations, to model ice nucleation on substrate surfaces have yet not yielded a defined set of requirements that make up an INAS [*Knopf et al.*, 2018; *Knopf et al.*, 2020]. As outlined below, however, application of microanalysis techniques has made progress in identifying the physicochemical surface features that are involved in initiating ice nucleation on substrate surfaces.

1.3 Ice crystal habits, morphology, growth, and sublimation

Subsequent to ice nucleation on the nanoscale, ice crystals grow in the humidified environment to larger sizes reaching up to snowflake dimensions that are observable with a typical optical microscope (OM) [*Bentley and Humphreys*, 1931; *Libbrecht*, 2005; *Nakaya*, 1954]. However, before ice crystals sediment via precipitation, the formation of micrometer-sized ice crystals and their altering morphologies under super- and subsaturated conditions impact cloud albedo and thus the climatic effect of clouds. It is well known that the shape of cirrus ice particles can have a profound impact on Earth's radiation budget [*Hartmann*, 2016; *Jensen et al.*, 2009; *Lawson et al.*, 2019; *McFarquhar et al.*, 2002; *Mishchenko et al.*, 1996]. For example, the differences in ice crystal shapes can lead to differences in the up- and downwelling infrared irradiance of cirrus clouds by tens of Watts per m^2 [*Wendisch et al.*, 2007].

Ice crystal shapes depend on the environmental conditions T and RH [*Bacon and Swanson*, 2000; *Bailey and Hallett*, 2002; 2004; *Bailey and Hallett*, 2009; *Pruppacher and Klett*, 1997]. Figure 4 displays the various ice crystal habits obtained from laboratory studies and field campaigns that develop for changing conditions in parameters T and S_{ice} [*Bailey and Hallett*, 2009]. As evident in Fig. 4, as temperature decreases the regime of single crystals moves into the polycrystalline habits where at greater temperatures plate-like and at lower temperatures

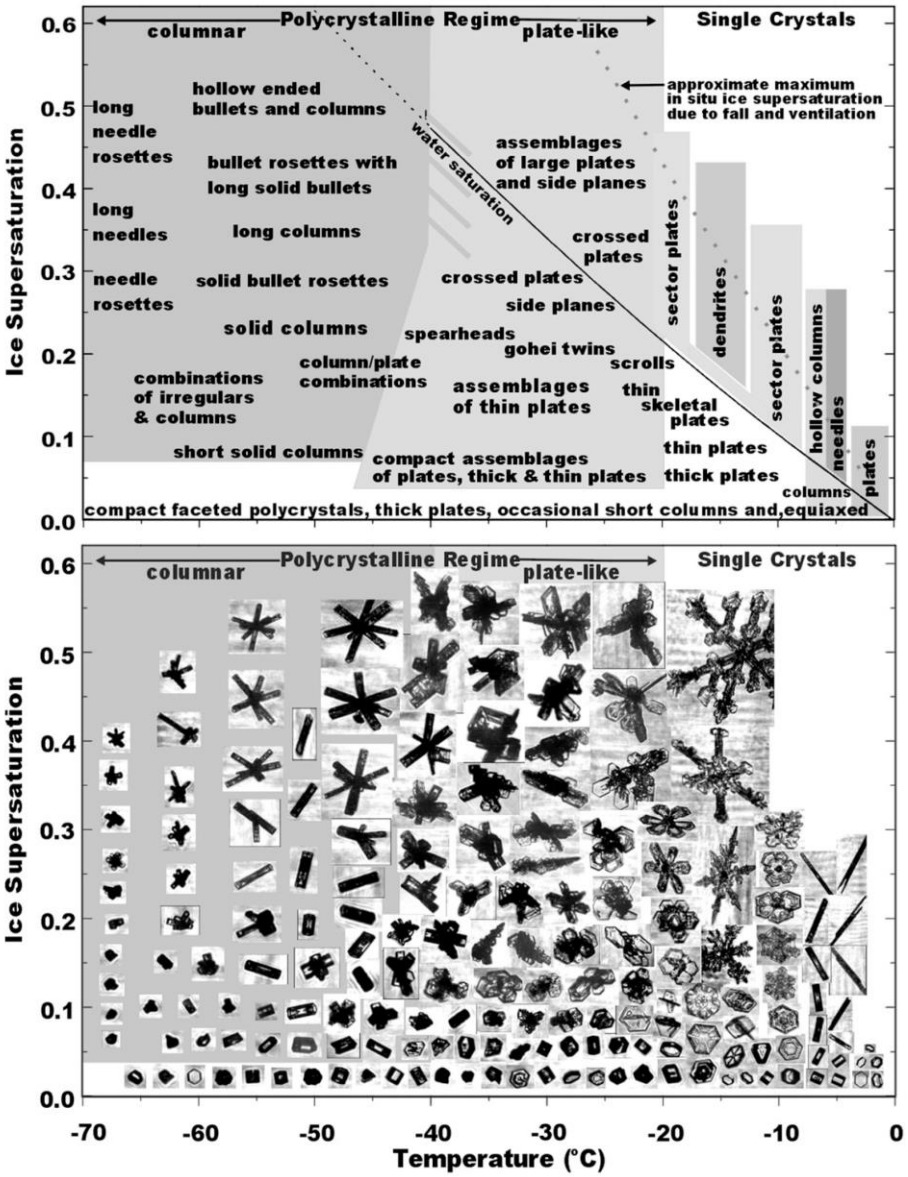

Figure 4. Ice crystal habit diagram derived from laboratory and field campaign observations as a function of temperature and ice supersaturation. From *Bailey and Hallett* [2009].

columnar ice crystals dominate. Increases in S_{ice} can change crystal habits ranging from compact, thick, and thin plates to bullet rosettes and hollow ended bullets. Figure 4 exemplifies the complexity of ice crystal growth and its ramifications for cloud and climate modeling.

Ice crystal and snowflake morphologies have been traditionally studied by OM, but in recent years environmental scanning electron microscopy (ESEM) has been applied to growing and sublimating ice crystals demonstrating, by use of greater resolution, a complex picture of linear striations, ridges, islands, steps, peaks, pits, and crevasses on the facets of the ice [*Magee et al.*, 2014]. *Magee et al.* [2021] also examined cirrus ice particles using ESEM corroborating previous ice habit studies, though the higher resolution examination of ice crystals points to an even greater particle complexity as shown in Fig. 4.

Microscopic understanding of ice surfaces, including premelted layers of ice, affects many environmental processes including growth rates and shapes of snowflakes, the sintering of snowfields, transport of impurities along grain boundaries, and thunderstorm lightning [*Dash et al.*, 2006]. Grain boundaries represent the interface between individual ice crystals. These grain boundaries change when ice crystals grow, melt, or sublimate [*Cascajo-Castresana et al.*, 2021; *Pedersen et al.*, 2011; *Pfalzgraff et al.*, 2010]. These processes, in turn, influence ice crystal shape, its interaction with adsorbing and reactive gas species (e.g., heterogeneous reactions), and distribution of species expelled during ice growth [*Bogdan*, 2018; *Bogdan and Molina*, 2017; *Zobrist et al.*, 2008].

When ice forms from an aqueous solution, the ice crystal expels solutes, thereby generating a concentrated solution, that is subsaturated with respect to ice. Figure 5 displays this process schematically [*Bogdan*, 2018]. The remaining solution, also termed freeze-concentrated solution (FCS), may coat the ice crystal. Under atmospheric ice forming conditions, the FCS will take up

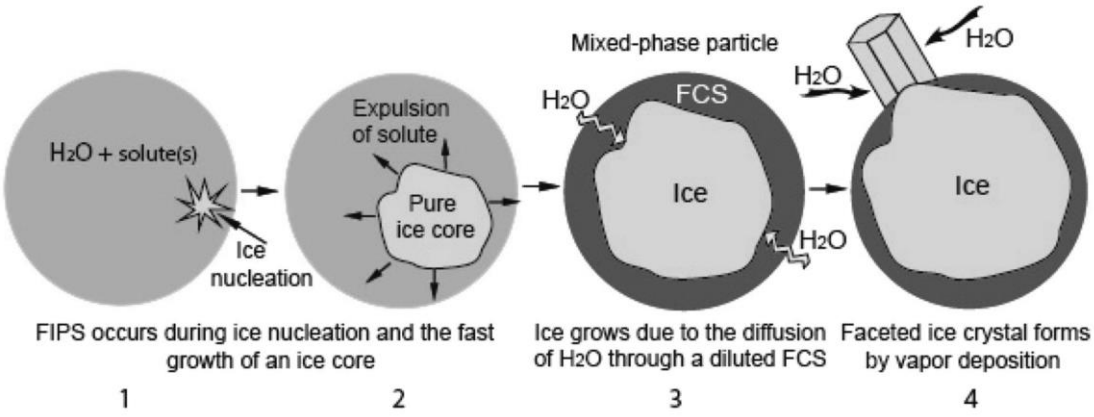

Figure 5. Sequences that can lead to the formation of a freeze concentrated solution (FCS) surrounding an ice crystal (1-3). Water vapor may be taken up by the FCS allowing the ice crystal to further grow from the diluted FCS (3). As the ice crystal disrupts the FCS, it may serve as a deposition INP (4). From *Bogdan* [2018].

water, leading to further ice crystal growth, which then potentially acts as a nucleation site of ice formation by vapor deposition. These processes, which are especially relevant at higher altitudes and colder temperatures where freezing from aqueous solution droplets is more likely, have only received limited attention. Furthermore, these initial studies are restricted to OM [*Bogdan*, 2018; *Bogdan and Molina*, 2017; *Bogdan et al.*, 2016].

2 Application of microanalysis techniques to study ice formation

During the last two to three decades, the field of atmospheric ice nucleation has seen the application of various microanalysis techniques to deduce the occurrence of ice nucleation and to examine the INP or ice-nucleating substrate. The study of homogeneous ice nucleation typically employs optical microscopy for detection of the freezing of micrometer-sized droplets when temperatures are close to the homogeneous freezing limit [*Knopf and Lopez*, 2009; *Knopf and Rigg*, 2011; *Riechers et al.*, 2013; *Shardt et al.*, 2022; *Stan et al.*, 2009; *Tarn et al.*, 2021]. However, when aiming for deeper supercooling, reaching temperatures beyond the homogeneous freezing limit, nanodroplets generated by a supersonic nozzle allowing for rapid cooling rates are examined for freezing temperatures and rates [*Amaya and Wyslouzil*, 2018]. In these

experiments, e.g., Fourier Transform Infrared spectroscopy, and Small and Wide Angle X-ray Scattering (SAXS and WAXS, respectively) are applied to probe the droplet temperature, volume, crystallinity, and structure of ice [*Amaya and Wyslouzil*, 2018]. In the latter study, WAXS provided the ability to evaluate the ice structure indicating that the ice crystals formed at 218 K consisted of a mixture of hexagonal and cubic ice lattice structures.

The majority of the heterogeneous ice nucleation studies that make use of microanalysis techniques can be divided into two approaches: One is using a multi-instrumental, also termed multimodal, analytical approach [*Laskin et al.*, 2016; *Laskin et al.*, 2019] where ice formation is assessed with one type of instrument, not necessarily a microanalysis technique, and the corresponding INP or ice-nucleating substrate is subsequently interrogated by microanalysis methods discussed in this book. The other approach directly applies microanalysis techniques for in situ detection of ice nucleation. In this section, we will introduce both approaches with examples of procedures and setups.

The microanalysis techniques used in studies of ice nucleation and ice crystal growth include Raman, scanning electron microscopy with energy dispersive X-ray spectroscopy (SEM/EDX or SEM/EDS), transmission electron microscopy (TEM), atomic force microscopy (AFM), and scanning transmission X-ray microscopy with near-edge X-ray absorption fine structure spectroscopy (STXM/NEXAFS). Each of these techniques has its own requirements and limitations as discussed in the previous chapters. Relevant for studying the ice phase are sample substrates, resolution, field of view, radiation effects on sample, and achieving uniform T and RH fields. So far, only Raman, SEM/EDX, and STXM/NEXAFS have been applied for in situ detection of ice formation.

The different microanalytical approaches have different requirements for the supporting substrates of the sample that allows for introduction into the instrument. This can further complicate sample preparation when studying ice nucleation by particles deposited on a supporting substrate. For obvious reasons, the supporting substrate should not interfere with the observed ice nucleation. In other words, it must not be hygroscopic and must be a less efficient ice-nucleating agent compared to the investigated particles or materials deposited on the supporting substrate. For the case of OM and Raman application, hydrophobically coated glass or quartz slides have been shown to minimize heterogeneous ice nucleation, even allowing the study of homogeneous freezing of aqueous droplets [*Bertram et al.*, 2000; *Knopf et al.*, 2002; *Knopf et al.*, 2003; *Koop et al.*, 1998]. Silicon wafer substrates coated with a silicon nitride film are suitable for ice nucleation experiments and the application of SEM/EDX [*Knopf et al.*, 2014; *Wang et al.*, 2016]. The few ice nucleation studies utilizing STXM/NEXAFS demonstrate that silicon nitride-coated Si frames are also suitable for studying ice nucleation in a multimodal or in situ manner [*Alpert et al.*, 2022a; *Alpert et al.*, 2022b; *Knopf et al.*, 2014]. Nevertheless, due to the very thin membrane films associated with the silicon nitride-coated Si frames, handling and ice nucleation experiments can present a challenge for the experimentalist.

2.1 Multimodal microanalysis of ice nucleation

To gain an understanding of the nature of the INPs, studies focused early on the examination of ice crystal residuals (ICRs) by microanalysis techniques including TEM and SEM/EDX [*Chen et al.*, 1998; *Cziczo et al.*, 2004; *Heintzenberg et al.*, 1996; *Kreidenweis et al.*, 1998; *Petzold et al.*, 1998; *Twohy and Gandrud*, 1998]. Typically, in the first step, the ambient aerosol particles were activated to form ice crystals that continue to grow in a supersaturated environment, e.g., in a continuous flow diffusion chamber [*Rogers*, 1988]. In the second step, the ice crystals are size-

selected by an impactor for deposition on supporting substrates [*Chen et al.*, 1998; *Kreidenweis et al.*, 1998] or by a counter-flow virtual impactor (CVI) [*Cziczo et al.*, 2017; *Twohy and Gandrud*, 1998]. Application of these approaches, e.g., *Chen et al.* [1998] found that the INPs relevant for cirrus formation conditions in the upper troposphere can consist of crustal, sulfate, carbonaceous, metallic, and other unidentified materials. Clearly, these early studies using TEM and SEM advanced our understanding of the chemical complexity of atmospheric INPs.

During the Indirect and Semi-Direct Aerosol Campaign (ISDAC) near Barrow, Alaska, in spring of 2008 [*Hiranuma et al.*, 2013] collected ICRs using CVI (Fig. 6). The ICRs were examined by STXM/NEXAFS at the carbon K-edge to enable the speciation of the organic matter in resolution of tens of nanometers. Application of STXM demonstrated that ICRs possessed a thin organic coating composed of carboxylic functional groups (Fig. 6). Organic matter associated with INPs has been recognized to play an important role when determining sources of atmospheric INPs [*Knopf et al.*, 2018].

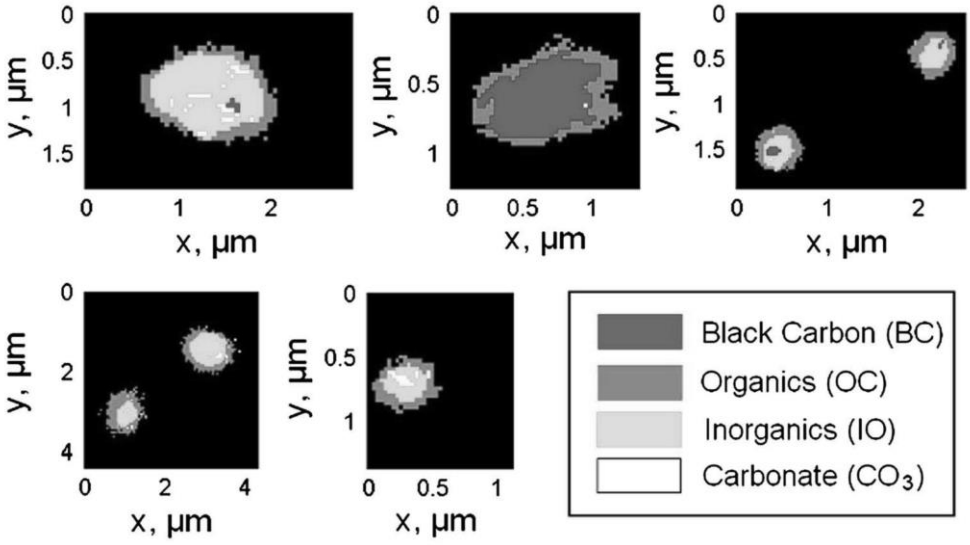

Figure 6. Ice crystal residuals (ICRs) collected during the Indirect and Semi-Direct Aerosol Campaign (ISDAC) by aircraft applying a counterflow virtual impactor (CVI). Panels show scanning transmission X-ray microscopy with near-edge X-ray absorption fine structure spectroscopy (STXM/NEXAFS) false color maps of the ICRs where the greyscale-related composition is given in the legend. The analysis indicates that the ICRs contain cores composed of inorganic, black carbon, and carbonate that are coated with organic matter. From *Hiranuma et al.* [2013].

Another common approach is to collect laboratory-generated particles or substrates and field-collected particles on substrates that allow for ice nucleation experiments and microanalysis using SEM/EDX and STXM/NEXAFS [*Alpert et al.*, 2022b; *Charnawskas et al.*, 2017; *China et al.*, 2017; *Holden et al.*, 2019; *Knopf et al.*, 2014; *Knopf et al.*, 2021; *Knopf et al.*, 2022; *Lata et al.*, 2021; *Wang et al.*, 2012a; *Wang et al.*, 2012b]. The ice nucleation experiments typically use a chamber, where the particle sample is located at the bottom on a temperature-controlled cold stage [*Dymarska et al.*, 2006; *Wang and Knopf*, 2011]. This stage defines the particle or supporting substrate temperature. The chamber is sealed against room air that allows for the introduction of a controlled humidified gas flow. Having control of particle T and RH permits simulation of typical atmospheric conditions, such as mimicking of atmospheric advection that results in cloud formation. As S_{ice} increases, water uptake, immersion freezing, and deposition ice nucleation can be observed microscopically. When adjusting the chamber RH to achieve subsaturated conditions, water evaporates or ice sublimates. An example of this procedure using OM for the ice nucleation experiment is outlined in Fig. 7. Application of OM typically allows for a greater field of view compared to SEM or STXM, thereby minimizing experimental artifacts such as ice formation outside of the field of view or at the fringes of the particle sample. Using this technique, radiation effects are negligible. Upon visual detection of ice formation, the particle sample area can be examined with greater magnification (Fig. 7a). Observation of the sublimation of the ice crystals allows for pinpointing the INPs that were the source of the ice crystal formation (Fig. 7b). Subsequently, using digital imaging analysis, the INPs can be relocated and imagined with greater resolution by the microanalysis instrumentation, here, a SEM (Fig. 7c-e). In general, this multimodal approach allows for the morphological and chemical characterization of the particle or substrate area by SEM that initiated ice nucleation.

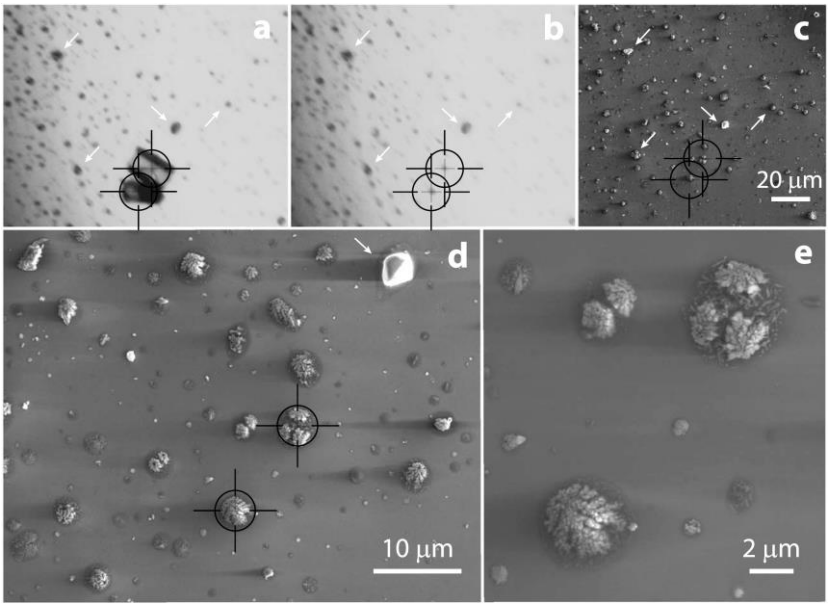

Figure 7. Multimodal identification of ice-nucleating particles (INPs) using optical microscopy (OM) and scanning electron microscopy (SEM). a: The cross hairs display the position of the center of ice crystals as determined by OM. b: Subsequent to ice crystal sublimation, the cross hairs indicate the location of INPs. c: The same field of view as in (b) imaged by SEM. d and e: Application of higher magnification using SEM to image in-detail morphology of identified INPs. The white arrows point to the same particles in (a) to (d). From *Knopf et al.* [2014].

The identified INPs, shown in Fig. 7, are not different from other adjacent particles located on the same substrate. They demonstrate similar size, morphology, and elemental compositions as determined by EDX (not shown) as the non-INPs.

In the same ice nucleation experiment, *Knopf et al.* [2014] used STXM/NEXAFS to analyze INPs and non-INPs deposited on silicon nitride-windows, which consist of a 100 nm thin film supported by a Si frame. The experimental challenge during the experiments was to keep the supporting substrate temperature uniformly consistent between the thin film and Si frame to avoid ice nucleation artifacts. Figure 8 shows a multimodal microanalysis study of ambient particles acting as INPs using OM, SEM, and STXM [*Knopf et al.*, 2014]. Figure 8A and B show an image of aerosol particles as dark light absorbing spots dispersed over the silicon nitride window as the bright grey square and the supporting Si frame as darker grey area as visualized by OM. Panel (A) shows the emergence of an ice crystal during supersaturated conditions. Panel

(B) represents the sample in (A) after sublimation of the ice crystal. Panel (C) shows the area in (A) where ice formed in greater resolution using SEM. The sample was subsequently transferred to STXM/NEXAFS to chemically speciate the organic components using the carbon K-edge (panels D to G). False-grey color images of the INP (D) and non-INPs (E, F) reveal the presence of inorganic species (darkest grey color), calcium (brightest grey color), and organic carbonaceous (intermediate grey color) matter. The INP is completely surrounded by the organic carbonaceous matter. The absorption spectrum shown in panel (G) indicates that in areas dominated by inorganic species or calcium, organic functionalities are present, here COOH groups. Hence, in panels D to F, dark grey and brightest grey represent areas that are dominated

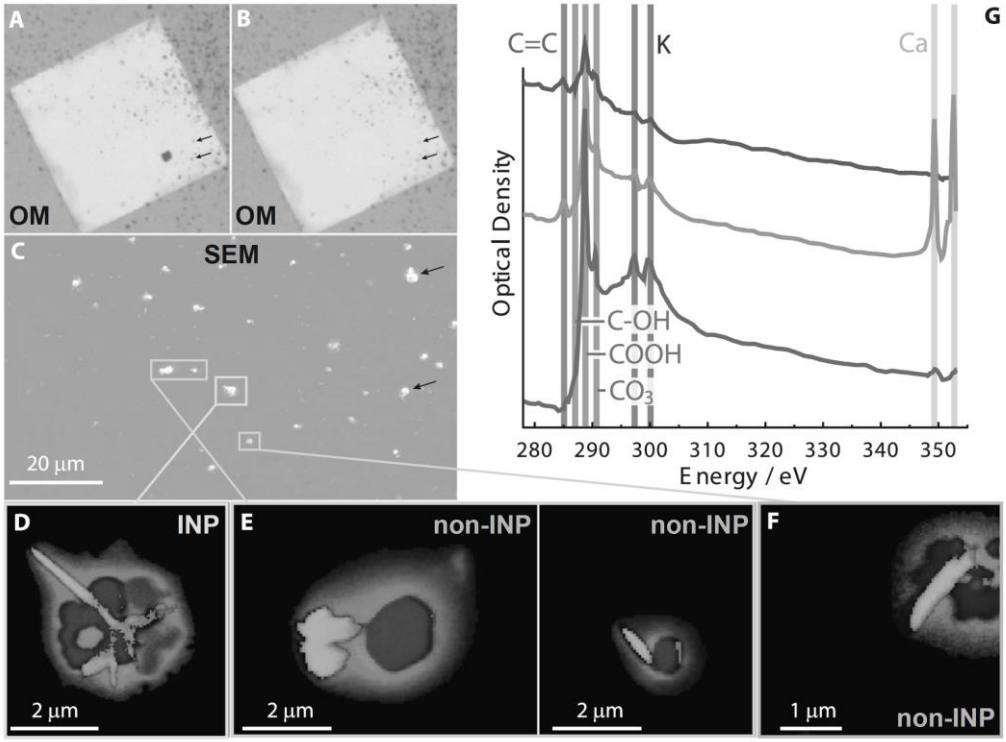

Figure 8. Ice-nucleating particle (INP) identification and scanning transmission X-ray microscopy with near-edge X-ray absorption fine structure spectroscopy (STXM/NEXAFS) chemical imaging of particles. A and B: Ice formation and ice sublimation events observed in the OM experiment. C: Scanning electron microscopy (SEM) image of the same sample area at higher magnification. The black arrows point to the same particles in A to C. D: Identified INP. E and F: Non-INPs. The component images in D to F emphasize the contrast between non-carbonaceous inorganic species (darkest grey color), organic carbonaceous (intermediate grey color), and calcium (brightest grey color). G: NEXAFS spectra of the dominant particle regions (inorganic, calcium, and organic) with the major functionalities highlighted. Adapted from [*Knopf et al.*, 2014].

by inorganic species (due to absorption through the entire particle) but that are also coated by OC matter. Panels D to F also demonstrate that within a resolution of about 30 nm, the INP and non-INPs cannot be physicochemically distinguished, thereby corroborating SEM/EDX observations.

The application of multimodal microanalytical techniques to study ice nucleation significantly advances our understanding of atmospheric ice crystal formation. The observations clearly demonstrate that organic matter is associated with INPs. However, which physicochemical properties of the organic matter, including the presence of certain organic functionalities, surface morphology, or phase state, serve as the ice-nucleating agent or an INAS has yet to be resolved. The presence of organic matter corroborates previous CVI-based collection and chemical characterization of ICRs. Furthermore, microanalytical studies that examine the particle population on a statistical significant level and associated INPs find that the INPs cannot be physicochemically distinguished from the dominant particle types (i.e., non-INPs) in the particle population present on the substrate [*Alpert et al.*, 2022b; *China et al.*, 2017; *Knopf et al.*, 2014; *Knopf et al.*, 2022; *Lata et al.*, 2021; *Wang et al.*, 2012b]. This emphasizes the previous point, which concerns the microscopic nature of the surface feature or INAS, which ultimately facilitates ice nucleation. Although the INP can be chemically imaged, its surface area is still orders of magnitude larger than the likely point of ice nucleation. Furthermore, the various multimodal approaches cannot resolve where on the particle ice nucleation commenced since ice formation is not monitored in situ. Despite these caveats, multimodal physicochemical characterization and chemical imaging of aerosol particles and INPs greatly advance our understanding of atmospheric ice formation. By learning the physicochemical properties of INPs, the role of chemical and physical aging of particles during atmospheric transport for ice nucleation and the sources and emissions of aerosol particles that potentially act as INPs can be

assessed, thereby improving ice crystal formation in cloud and climate models [*Kanji et al.*, 2017; *Knopf et al.*, 2018].

In recent studies, Friddle and Thürmer combined an OM with an ice nucleation cell that allows for control of substrate temperature and humidity. In addition, an AFM for visualization

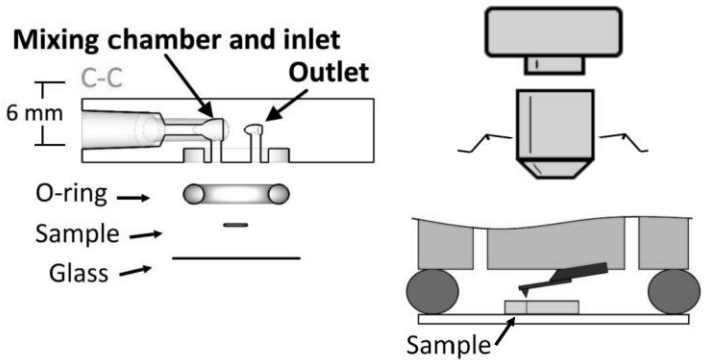

Figure 9. Collocated optical microscopy with atomic force microscopy (AFM) coupled to a micro-mixing chamber for humidity control and a cold stage at the bottom to control the temperature of the sample. Adapted from *Friddle and Thürmer* [2020].

was integrated into this setup to sequentially examine the role of nano-surface steps promoting ice formation on feldspar [*Friddle and Thürmer*, 2019; 2020]. Figure 9 shows a schematic of the OM-ice nucleation-AFM setup. A mixing chamber provides the desired humidity exposure of the sample. The sample is cooled by a cold nitrogen gas flow at the bottom of the cell, not shown here. An OM is used to visually detect water condensation and ice formation. An AFM is integrated into the top of the mixing cell. Figure 10 provides an example of an ice formation experiment where OM and AFM are collocated. This experiment indicates that ice formed on a small protrusion located on the feldspar surface. As the authors point out, the INAS cannot be directly determined due to limited resolution [*Friddle and Thürmer*, 2020]. For example, the scale of the identified protrusion (Fig. 10e) is larger than most atmospheric particles. During this experiment, ice was observed to rapidly spread stepwise along the feldspar surface. At -30 °C the number of ice-bearing steps was related to step height and humidity [*Friddle and Thürmer*, 2019]. Though humidity levels applied in these experiments reflect greatly supersaturated

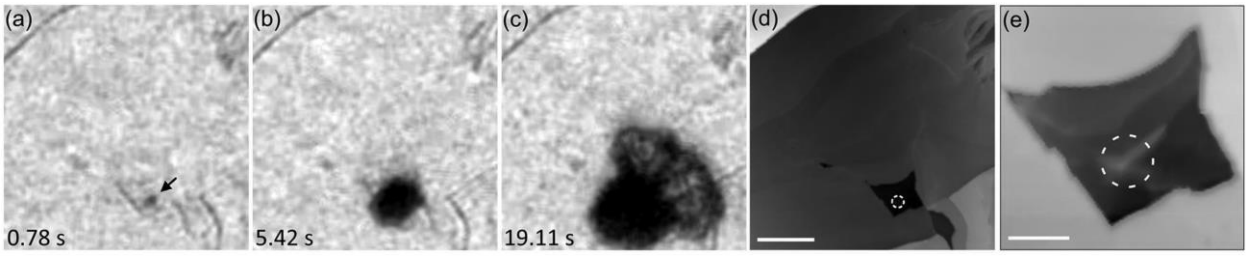

Figure 10. Ice formation on feldspar surface at -29.5 °C observed with optical microscopy (OM) (panels a to c) and collocated atomic force microscopy (AFM) topography (panels d and e). (d) AFM image of the same location in (a)–(c) with dashed circle around the area of nucleation. The scale bar indicates 20 μm. (e) Expanded view of the identified area of nucleation in (d) depicting a small protrusion within a larger pit. The scale bar represents 5 μm. Adapted from *Friddle and Thürmer* [2020].

conditions with respect to water, S_{water}. The step height decreases with increasing S_{water}. For example, at -30 °C for a 50% chance of a step bearing ice, a step must be taller than 1 μm at S_{water} = 1.32 but can be as small as 14 nm at S_{water} = 2.32 [*Friddle and Thürmer*, 2019]. Typically, maximum S_{water} achieved in the atmosphere is about 1.04. How a step size of about 1 μm translates to sub- and supermicrometer-sized particles remains an open question. However, it cannot be ignored that ice was observed preferentially at steps, and so this multimodal analytical study shows that step-like features may play a role in ice formation via initial water condensation on feldspar surfaces. More research is needed to establish how such findings translate to particles that are smaller than those identified features and if ice nucleation commences for lower S_{water}.

2.2 In situ microanalysis of ice nucleation

Examination of ice nucleation by in situ methods involves experimental setups that couple temperature and humidity control of the particle and substrate sample with the desired microanalysis technique. Raman, SEM, and STXM have been employed to examine ice nucleation in situ. Similar to the multimodal approach discussed in the previous section, the supporting substrate on which particles are deposited onto needs to satisfy the instruments requirements and show lower water uptake and ice nucleation efficacy compared to the sample that is being examined.

2.2.1 Raman spectroscopy to study ice nucleation

Raman spectroscopy is often used along with OM, making it an excellent choice to monitor phase transitions of particles including ice nucleation and chemical composition of aerosol particles and INPs. Raman spectroscopy to study particle phase transition is currently limited to particles diameters of about 1 µm due to typically applied excitation wavelengths. Although surface-enhanced- and tip-enhanced Raman spectroscopy [*Bailo and Deckert,* 2008; *Campion and Kambhampati*, 1998; *Cialla et al.*, 2012; *Zrimsek et al.*, 2017] can reach resolutions in the tens of nanometers, these techniques have yet not been applied to study ice nucleation in situ.

A custom-built cold stage applying confocal Raman spectroscopy was designed to detect the crystallization of aqueous HNO_3 solution droplets forming nitric acid dihydrate and nitric acid trihydrate representing a type of polar stratospheric clouds [*Knopf et al.,* 2002]. The same Raman-OM setup was subsequently applied to examine changes in composition and ice formation in aqueous $(NH_4)_2SO_4$ and H_2SO_4 droplets [*Knopf et al.,* 2003]. When applying Raman spectroscopy, care has to be taken that the laser light does not significantly warm the particle of interest. This could result in composition changes and erroneous freezing temperatures. For example, *Knopf et al.* [2003] monitored potential changes in the recorded vibration bands when exposing the droplets to different excitation time periods and using different laser powers. Additionally, they measured the melting point of the aqueous droplets to infer potential heating due to laser radiation. For aqueous systems these issues may be minor but when investigating absorbing species such as soot or certain mineral dust species, the sample or particle can significantly heat up and alter the thermodynamic conditions for nucleation (i.e., S_{ice}).

The study of atmospheric ice nucleation has involved the coupling of ice nucleation cells or environmental cells to Raman-OM where particles or substrate can be temperature-controlled and exposed to desired levels of humidity and, in some cases, reactive gases such as ozone [*Baustian et al.*, 2012; *Baustian et al.*, 2013; *Baustian et al.*, 2010; *Knopf and Koop*, 2006; *Mael et al.*, 2019; *Roy et al.*, 2021; *Schill and Tolbert*, 2013; *Wang and Knopf*, 2011]. Figure 11a provides an example of a setup that allows exposure of deposited particles to different humidity levels and reactive gases while controlling the particle temperature [*Mael et al.*, 2019]. A

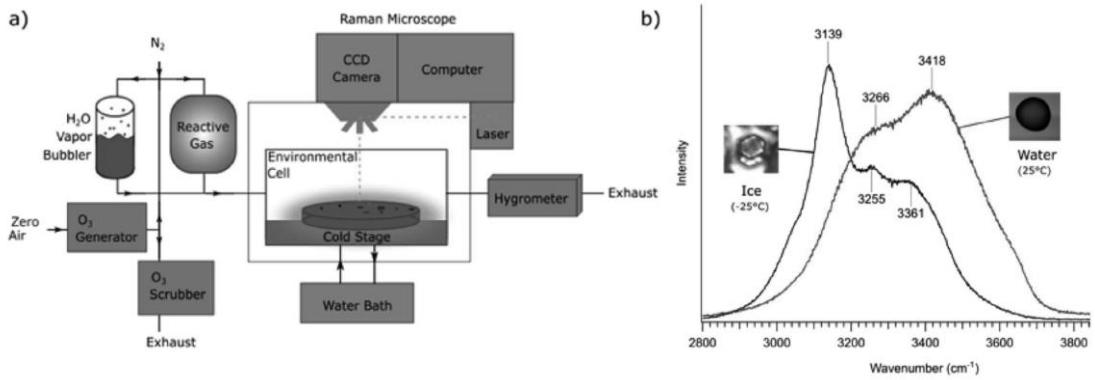

Figure 11. Raman microscope application to study ice nucleation. (a) An environmental cell allowing for control of temperature of deposited aerosol particles (cold stage) and gas humidity is coupled to the Raman microscope. Humidity within the environmental cell is adjusted by mixing a dry and saturated flow of nitrogen. In addition, reactive gases can be introduced into the cell. (b) Raman spectra and corresponding optical images of ice and water at −25 and 25 °C, respectively. From *Mael et al.* [2019].

humidified flow is typically generated by mixing a dry flow of an inert gas such as N_2 with a saturated N_2 gas flow. A hygrometer at the exit of the environmental cell's gas flow is applied to measure the dew point and as such the water vapor amount present in the cell [*Dymarska et al.*, 2006; *Mael et al.*, 2019; *Wang and Knopf*, 2011]. As indicated in Fig. 11b, OM allows visual inspection of the droplet or ice crystal in addition to in situ compositional examination by Raman spectroscopy.

Recording of Raman maps allows identification of the INP and its surface features that initiated heterogeneous ice nucleation [*Schill and Tolbert*, 2013; 2014]. For example, *Schill and*

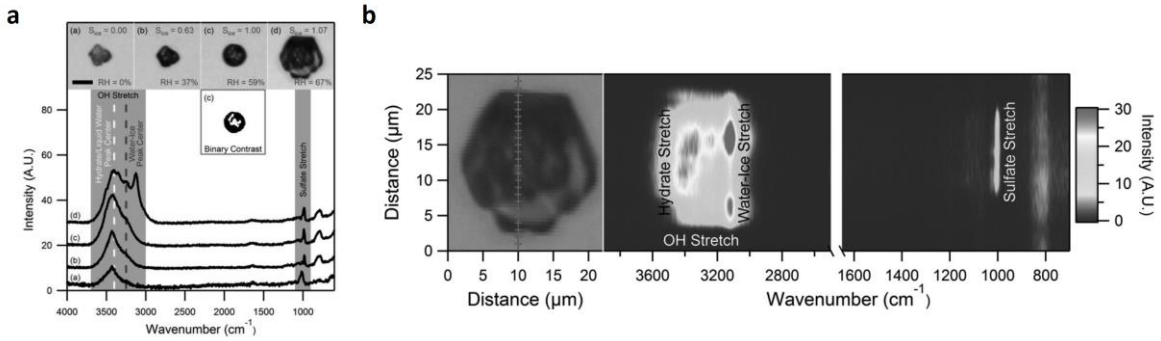

Figure 12. Immersion freezing from a synthetic sea-salt (SSS) particle as humidity is increased. (a) Images of a synthetic sea-salt (SSS) particle ranging from dry conditions until ice nucleation occurred. The size bar represents 10 μm. The corresponding Raman spectra are shown below the optical images. (b) Detailed Raman spectra line maps of the frozen particle shown in (a) recorded along the crossed line. The SSS particle serves as immersion freezing INP, being at the center of the frozen particle as indicated by the hydrate and sulfate stretches being only present in the center region. Adapted from *Schill and Tolbert* [2014].

Tolbert [2013] demonstrated that ice formed from the supersaturated gas phase on a spherical and glassy organic droplet. Another example is given in Fig. 12 where synthetic sea-salt particles were exposed to conditions $S_{ice} > 1$ [*Schill and Tolbert*, 2014]. Water uptake and freezing can be clearly identified in the visual recording and in the associated Raman spectra (Fig. 12a). This further corroborates that ice nucleation commenced in the immersion freezing mode. The corresponding line scan of the ice crystal (Fig. 12b) corroborates that the immersion freezing INP resides in the center of the ice crystal. Only the center of the line scan shows hydrate and sulfate peaks representative of the INP.

2.2.2 ESEM in situ ice nucleation experiments

Environmental scanning electron microscopy (ESEM) allows particles and uncoated biological and other materials to be examined in a high-pressure (up to 60 hPa) chamber with an electron beam. The gas introduced into the chamber can be water vapor, thereby opening the door for examination of environmental species and simulation of cloud forming conditions. Reviews on the application of ESEM in material sciences and for studying the ice phase are provided by [*Zhang et al.*, 2020] and [*Pach and Verdaguer*, 2022].

Zimmermann et al. [2007] introduced the first application of ESEM to study heterogeneous ice nucleation. They examined silver iodide and two clay minerals for their propensity to induce condensation freezing and deposition ice nucleation. The pressure in the chamber was equal to the water partial pressure. The lowest particle temperature examined was 250 K due to the limited regulation of the water partial pressure by the ESEM. Cooling of the substrates was achieved by means of a Peltier element. Calibration of T and RH was performed by determination of deliquescence RH of various salts at different temperatures. This pioneering study reproduced previous ice nucleation literature data. The authors noted that in some cases activation of particles to form ice was not reproducible, i.e., in each experimental run using the same particle sample, different particles induced ice nucleation. Also, the activated fraction of particles could not be precisely determined since only a small part of the supporting substrate was imaged at the magnifications applied.

These ESEM ice nucleation studies [*Zimmermann et al.*, 2007; *Zimmermann et al.*, 2008] initiated further development of ESEM as a tool to examine the phase transition and ice formation by atmospheric particles. *Wang et al.* [2016] developed an ice nucleation (IN)-ESEM platform, shown in Fig. 13, that allows simulation of cloud formation for temperatures as low as 190 K. With this setup, cirrus cloud conditions and polar stratospheric cloud formation can be investigated. Cooling of the sample is achieved using a cryo-cooling stage operated with liquid nitrogen (Fig. 13A). The entire cryo-cooling stage within the ESEM chamber is insulated and supply lines are evacuated to ensure that no water vapor condenses on the cryo-cooling stage and within the ESEM chamber except for the sample area (Fig. 13B). The coldest spot is only the 0.2 mm^2 sample area. Avoiding water condensation outside the field of view ensures that no water vapor pressure gradients and thus erroneous RH fields can establish. The amount of water partial

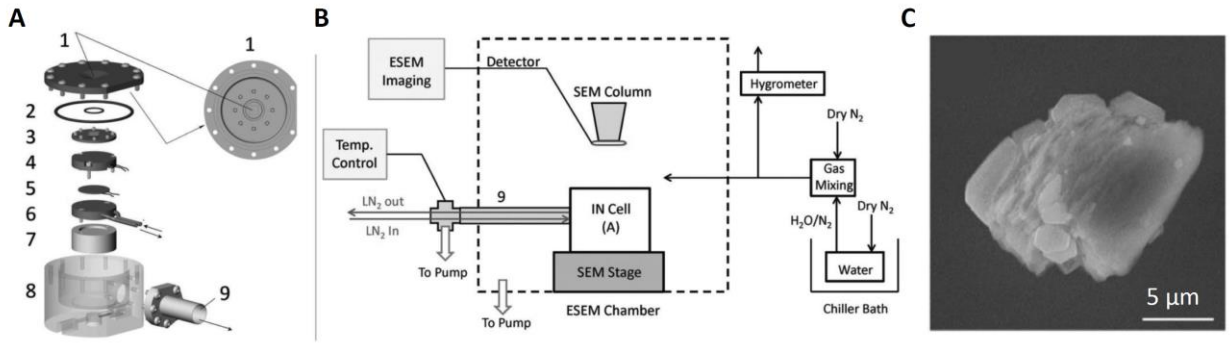

Figure 13. Ice nucleation cell implementation in an environmental scanning electron microscope (IN-ESEM). (A) provides a detailed schematic of the ice nucleation cell and (B) the displays the overall experimental layout of the IN-ESEM system including the IN cell within the ESEM chamber and a water vapor source (shown to the right) to control the chamber humidity. (C) presents observed deposition ice nucleation by kaolinite clay mineral where ice is depicted in brighter grey and the mineral in darker grey colors. Adapted from *Wang et al.* [2016].

pressure in the ESEM chamber is independently controlled by a gas flow system that allows mixing of a dry and humidified gas flow of N_2. The dew point of this gas mixture is continuously monitored by a chilled mirror hygrometer. Temperature and humidity were calibrated by measuring melting points of organic compounds and sublimation and growth of ice, respectively. Figure 13C shows exemplary deposition ice nucleation by a kaolinite clay mineral particle. Ice forms preferentially on the edges of the stacked kaolinite platelets and not on their basal planes. The authors suggest that the OH terminated edge surfaces of kaolinite platelets are potential ice nucleation sites [*Wang et al.*, 2016]. Thus, the chemical differences between the edge and the basal plane surfaces might have contributed to their different propensities to nucleate ice.

In Fig. 14 the ability of IN-ESEM to determine the thermodynamic conditions for ice nucleation initiated by kaolinite clay mineral via immersion freezing and deposition ice nucleation is demonstrated [*Wang et al.*, 2016]. The measurements are in agreement with previous OM based measurements [*Knopf et al.*, 2010; *Wang and Knopf*, 2011]. Since the entire sample area can be monitored, this IN-ESEM setup allows for INP identification and tracking when repeating ice nucleation experiments. Hence, it allows for a multimodal analytical

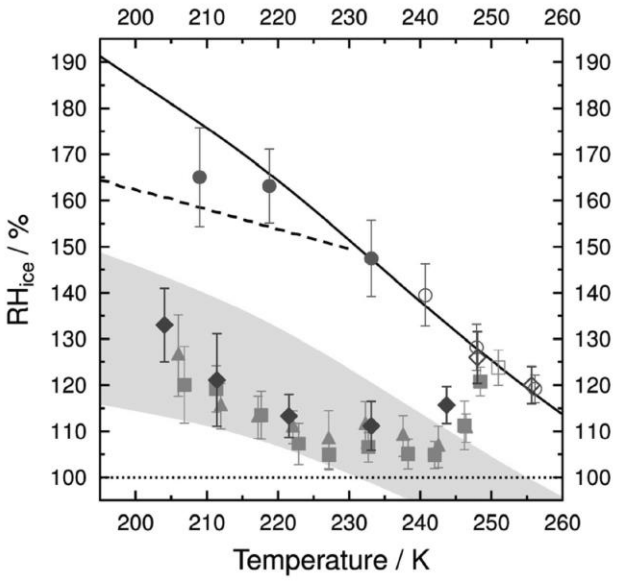

Figure 14. Deposition ice nucleation and immersion freezing by kaolinite clay minerals using the ice nucleation cell coupled to environmental scanning electron microscope setup (IN-ESEM) (solid and open diamonds, respectively) are given as a function of particle temperature and relative humidity with respect to ice (RH_{ice}). Observed ice formation and water condensation on blank substrates are given as solid and open circles, respectively. Grey symbols display previous literature values derived using optical microscopy (OM) [*Knopf et al.*, 2010; *Wang and Knopf*, 2011]. Conditions for pore condensation freezing by pores 7.5 – 15 nm in size are depicted by the shaded area [*Marcolli*, 2014]. Solid, dotted, and dashed lines indicate the water saturation (RH = 100%), ice saturation, and homogeneous ice nucleation limit [*Koop et al.*, 2000], respectively. From *Wang et al.* [2016].

approach. In addition to the IN-ESEM experiments, *Wang et al.* [2016] chemically imaged the identified INPs using STXM/NEXAFS and applied Helium ion microscopy to infer the role of pores in deposition ice nucleation (shaded area in Fig. 14). Although this study clearly identified kaolinite platelets as the location of ice nucleation thereby advancing our understanding of which surface features enable ice nucleation, in situ observation of an INAS was not possible.

In an ice-nucleating substrate-based study, *Kiselev et al.* [2017] equipped an ESEM with a custom-built cold-stage and water vapor supply system to study ice nucleation by potassium-rich feldspars. The cold-stage is a double-stage Peltier element coupled to the cold-water chiller allowing temperatures as low as 213 K to be reached. The cold sample area within the ESEM chamber is 5 × 5 mm^2 in size and the field of view in these experiments is maximum 700 µm in diameter. *Kiselev et al.* [2017] did not determine the ice nucleation onset S_{ice} from the pressure

or dew point measurements but rather from measurements of the ice crystal growth rates. As shown in Fig. 15A and B, ice nucleates in the vicinity of defect sites such as steps, cracks, and inside cavities on the (001) feldspar crystal face. In Fig. 15C an ice crystal forms on the (100) face of feldspar. This study shows that ice forms preferentially on high-energy (100) surface planes of feldspar. The location of ice crystals in Figs. 15A and B can be attributed to (100) faces being exposed in cracks and cavities. Accompanying molecular-scale computer simulations corroborate that the stable face of ice on the feldspar (100) surface is the primary prismatic plane [*Kiselev et al.*, 2017]. The (100) face of feldspar is hydroxylated and, thus, similar to the case of ice nucleation of on hydroxylated side planes of kaolinite, surface OH-groups seem to affect the ice nucleation propensity. This study clearly demonstrates the importance of the (100) face of feldspar for understanding of its ability to initiate heterogeneous ice nucleation. However, similar to other SEM-based ice nucleation studies the resolution is still too low to pinpoint unambiguously, the exact location where the critical ice nucleus interacts with the mineral surface. Some of the identified features, e.g., steps in cleaved surfaces, are larger than typical atmospheric particles. Hence, how many patches of the (100) face will be present on those much

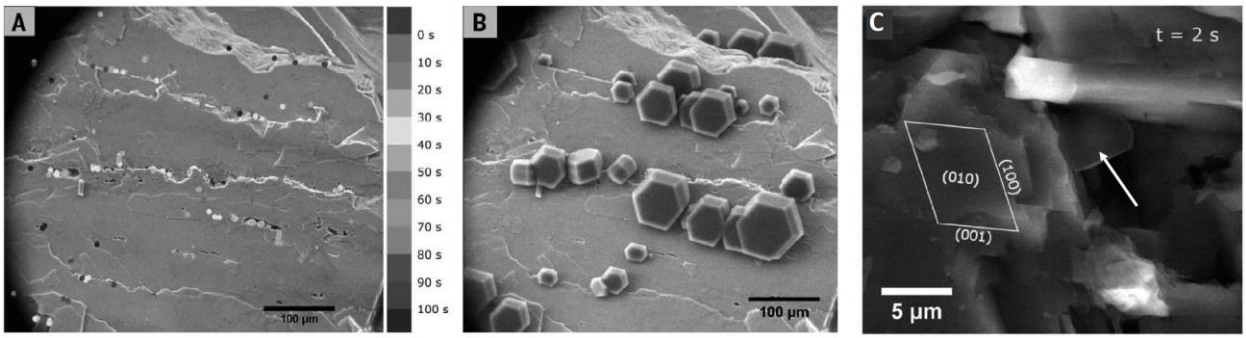

Figure 15. Application of an environmental scanning electron microscope (ESEM) equipped with a cold-stage to study the heterogeneous ice nucleation on (001) face of feldspar weathered in carbonated water. (A) Identification of ice nucleation sites from several nucleation-evaporation cycles, plotted over the image of the bare feldspar face. The greyscale color code gives the time of nucleation (in seconds) with respect to the first detected ice crystal. The grey arrow (above the scale bar) shows the location of the initial ice formation event that repeatedly occurs in all cycles. (B) Snapshot of the ice crystals nucleated at 233 K in the first nucleation evaporation cycle. C: Nucleation of an ice crystal (white arrow) on the inner wall of a cavity in the (010) face at 251 K. Adapted from *Kiselev et al.* [2017].

smaller feldspar containing particles? Would nanometer size resolution discover yet other features that explain the strong ice nucleation propensity of feldspar? How do the OH-groups interact with the adsorbing water and impact water structuring? Of course, these questions can be posed for any other application of microanalysis techniques to ice nucleation. It demonstrates that application of SEM significantly advances our understanding of the fundamental interactions between water and surfaces and as we achieve a closer look on ice nucleation more challenging and exciting research questions arise.

2.2.1 STXM in situ ice nucleation experiments

Soft X-rays by means of STXM have been successfully employed to observe in situ heterogeneous ice nucleation by mineral dust particles composed of either ferrihydrite or feldspar in presence or absence of organic matter including citric acid and xanthan gum [*Alpert et al.*, 2022a]. *Alpert et al.* [2022a] developed an in situ environmental ice cell or ice nucleation X-ray cell (INXCell), that can be mounted into a STXM instrument. The integration of INXCell within the STXM chamber is shown in Fig. 16. Key features of this design are the patterned temperature sensor on the surface of the silicon nitride membrane and a temperature-controlled ordering selecting aperture (OSA) which cools the particle sample area with a jet of cooled N_2. The temperature sensor is located at exactly at the same location as the deposited particles. To ensure that only the particle sample area is the coldest spot with uniform temperature in this setup, the INXCell and the particle sample are cooled separately. By guiding a cooled N_2 jet towards the particle sample area that is about 1-2 K colder than the temperature-controlled INXCell, the particles on the membrane inside, and not the silicon frame, are guaranteed to experience the coldest temperature. The INXCell has two membranes that seal the cell against the STXM vacuum chamber that is maintained at ~10^{-3} hPa whereas inside the humidified environment of

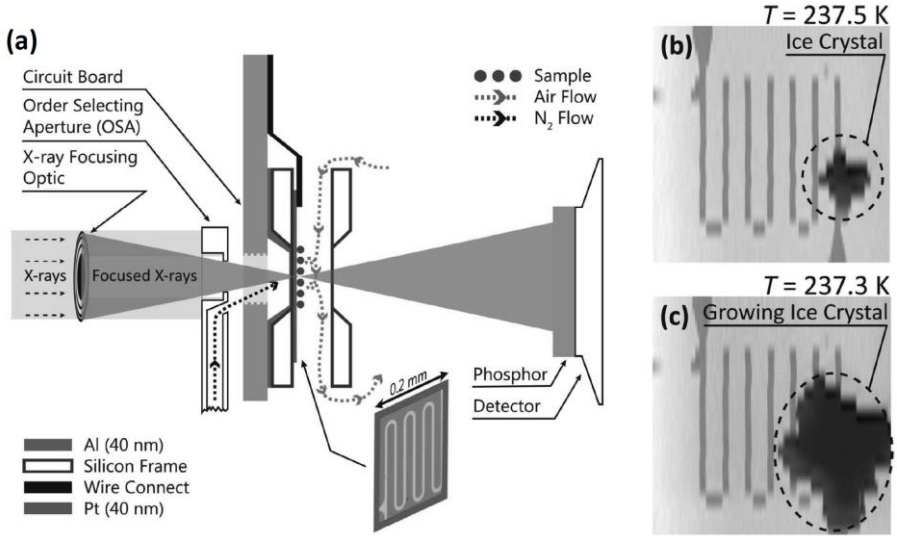

Figure 16. (a) Schematic configuration of the ice nucleation X-ray cell (INXCell) within the scanning transmission X-ray microscopy (STXM) chamber. The order selecting aperture (OSA) is temperature controlled and cools a gas jet that impinges on the back of the sample holder. Particles inside the INXCell (circles) are exposed to humidified air and cooled by the impinging gas jet. The INXCell is mounted on a circuit board that is connected to the lithographically fabricated temperature sensor on the sample substrate with a thickness of 40 nm. An optical microscope image of this sensor is displayed. Transmitted X-rays were detected using a phosphor screen coupled with a photomultiplier tube (PMT). A 40 nm aluminum layer was condensed onto the reverse side of the sample membrane to increase the lateral thermal conductivity. (b) and (c) Coarse mode resolution X-ray imaging (the sample area is about 200 µm across) to track ice crystal growth. Vertical bars indicate temperature sensor within the membrane. Adapted from *Alpert et al.* [2022a].

the cell, the pressure is maintained at 150 hPa. Calibration of S_{ice} was performed similarly to methods applied in OM studies [*Alpert et al.*, 2011; *Wang and Knopf*, 2011] where the growth and sublimation of ice crystals are monitored to determine S_{ice} = 1. At this instance, the dew point in the INXCell equals the particle temperature.

Figure 16b and c display the emergence of an ice crystal that has formed from droplets containing ferrihydrite particles serving as INPs [*Alpert et al.*, 2022a]. At constant water partial pressure, cooling the sample by 0.2 K yields rapid ice crystal growth. For initial monitoring of ice formation, a coarser resolution might be used.

The ability to visualize the ice crystal and to conduct NEXAFS on the ice crystal residuals and non-ice nucleating particles is depicted in Fig. 17 [*Alpert et al.*, 2022a]. Ferrihydrite particles coated with citric acid served as INPs. The shrinking ice crystal was observed using a coarse

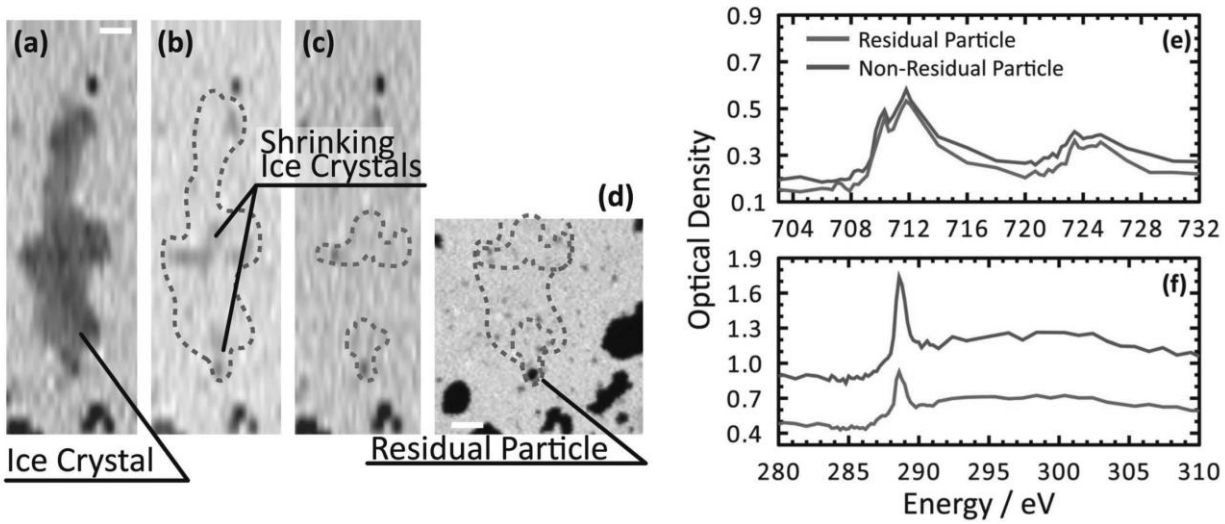

Figure 17. Observation of ice nucleation and spectroscopic identification of ferrihydrite particles coated with citric acid using scanning transmission X-ray microscopy with near-edge X-ray absorption fine structure spectroscopy (STXM/NEXAFS). (a)–(c) A sequence of X-ray images at 280 eV displaying a sublimating ice crystal. The dashed lines represent the ice crystal boundaries. (d) An X-ray image at 288.6 eV showing the ice crystal boundaries, residual particles after sublimation, and organic rich particles across the sample. The scale bar shown in (d) is 2 µm and valid for all images. NEXAFS spectra for an ice crystal residual particle and a non-ice nucleating particle recorded at the iron L2,3-edges shown in (e) and carbon K-edge shown in (f). Adapted from *Alpert et al.* [2022a].

resolution and carbon pre-edge energy of 280 eV to be sensitive to the presence of inorganic matter (Fig. 17 a and b). Subsequently a higher spatially resolved X-ray image is acquired at 288.6 eV, typical of carboxyl functional groups (Fig. 17 d). Figure 17e and f show NEXAFS spectra at the carbon K-edge and iron L2,3-edges, respectively, of the ice crystal residual particle and a particle that was not involved in ice formation, i.e., outside the marked area of the sublimating ice crystal (Fig. 17b-d). Both NEXAFS spectra show nearly identical spectral features indicating the presence of ferrihydrite (Fig. 17e) and citric acid with the carboxyl group at 288.6 eV (Fig. 17f). Given the resolution of ~35 nm in these experiments, no significant difference between the INP and non-INP is evident, a similar finding as in previous microanalytical studies of INPs [*Alpert et al.*, 2022b; *China et al.*, 2017; *Knopf et al.*, 2014; *Knopf et al.*, 2022; *Lata et al.*, 2021]. *Alpert et al.* [2022a] suggest that ice nucleation proceeded randomly with larger particles having a greater chance to serve as INPs than smaller particles.

These initial results using STXM to examine ice nucleation are an important step forward to advancing fundamental understanding of ice nucleation. The resolution of STXM is typically in the range of 20-50 nm meaning that it may just reach the upper limit of the surface area that determines the site of ice nucleation (Fig. 3). STXM will likely allow for higher resolution studies compared to SEM due to a lesser beam radiation effect on samples and water vapor. As in the case for OM- and SEM-based ice nucleation studies, a field of view to observe the entire cold sample is necessary. Consequently, instrument resolution need to be lower than what could actually be achieved, making sample configuration and characterization critical for high-resolution chemical imaging of ice nucleation.

The above examples demonstrate how microanalysis techniques have advanced our understanding of heterogeneous ice nucleation. Although the necessary resolution for monitoring the critical ice nucleus has not yet been achieved, the advancement of these microanalysis techniques has allowed us to identify physicochemical surface features and particle properties that contribute the ice nucleation ability of atmospheric particles. Ice nucleation by kaolinite and feldspar minerals depends on cracks, cavities, specific crystal lattice faces, and hydroxylated surfaces. Organic matter, rich in carboxyl functional groups, present in laboratory-generated and ambient atmospheric particles is involved in ice formation. INPs identified in ambient particle samples do not show unique physicochemical particle features compared to the majority of the particles in the sample. The same observation holds for laboratory-generated samples of inorganic/organic particles that serve as INPs. Although the study of INPs by microanalysis techniques is still in its infancy, the current results indicate that the search for the INP in a particle population is not one of finding the needle in the haystack but rather determining whether it is a larger or smaller piece of hay in the haystack. Clearly, it is too early for a

conclusion on this matter, thereby opening up exciting possibilities for new science in developing and applying microanalysis techniques to understanding of atmospheric ice nucleation.

3 Application of microanalysis techniques to study ice crystal growth and sublimation

ESEM has allowed the detailed study of ice crystal shapes under growth and sublimation conditions and when ice crystals contact each other [*Cascajo-Castresana et al.*, 2021; *Chen et al.*, 2017; *Magee et al.*, 2021; *Magee et al.*, 2014; *Nair et al.*, 2018; *Pach and Verdaguer*, 2022; *Pedersen et al.*, 2011; *Pfalzgraff et al.*, 2010].

Variable-pressure SEM obtained high-resolution images of growing and sublimating hexagonal ice surfaces presented by *Pfalzgraff et al.* [2010] show "growth strands" in the center of the prismatic face which get smoother towards its edges. During sublimation, however, "ablation strands" form on the prismatic face but close to its edge where there were deeper grooves. This study points out that the formation of ablation strands during ice crystal sublimation could result in greater reflectivity of cirrus clouds.

Using ESEM, *Nair et al.* [2018] examined sublimating ice crystals in detail. Under subsaturated conditions, the general sublimation behavior involved prismatic etch pits arising during the early stages, followed by ridge formation and the hollowing of basal planes. Figure 18 presents a suggested mechanism of the preferential crystallographic sublimation of an ice crystal that involves three key steps: initial random desorption, kink formation along the prismatic planes, and, finally, the subsequent ridge formation due to the coalescence of these kinks [*Nair et al.*, 2018]. Furthermore, the authors observed that the ridge length (λ_0 in Fig. 18) showed a power-law relationship with the pressure deviation from saturation. For less subsaturated conditions the ridge spacing was larger than for greater subsaturated conditions.

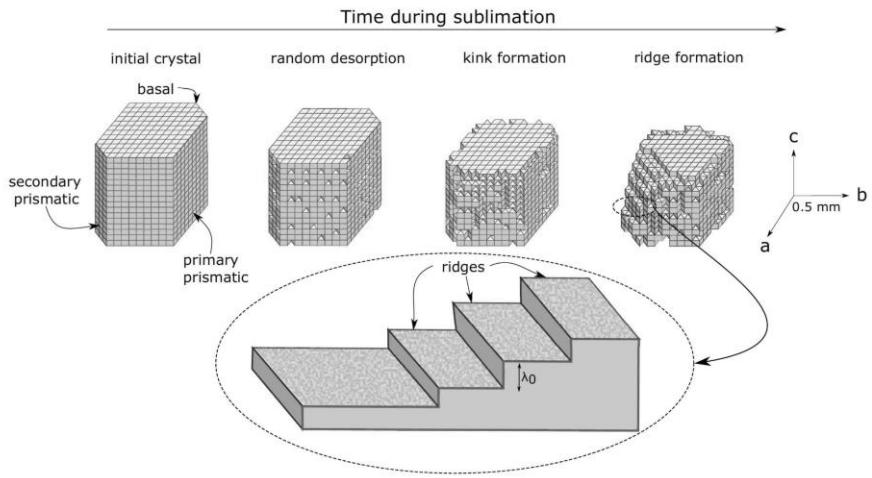

Figure 19. Conceptual mechanism to explain the preferential crystallographic sublimation on an ice crystal. This involves initial random removal of material, followed by sublimation of the basal planes resulting in the hollowing of etch pits parallel to the c axis. Kinks form since the sublimation along the secondary prismatic planes is thermodynamically less favorable. The kinks adjoining the basal and prismatic planes form as adatom mobility is impeded by the prismatic plane. Ultimately, these kinks coalesce to form ridges perpendicular to the basal plane with ridge length λ_0. The basal plane remains mesoscopically smooth. From *Nair et al.* [2018].

Pedersen et al. [2011] observed that when ice crystals grow in contact, they form an ice grain boundary that induces a surface transition on the facets in contact and does not propagate across the facet edges. A similar study by *Cascajo-Castresana et al.* [2021] observed the same phenomenon as shown in Fig. 19. These dislocations, appearing like grooves or waves, occur far (10 to 100 µm) from the contact point of the two growing ice crystals. *Pedersen et al.* [2011] interprets these observations as an "avalanche of dislocations" propagating away from the original dislocation. This viewpoint is supported by the theory of dislocation-mediated melting

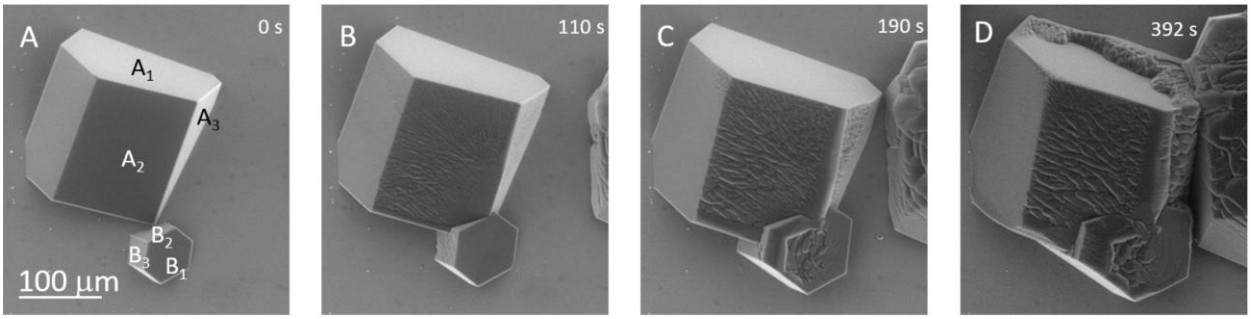

Figure 18. Ice crystal morphology changes upon merging of isolated crystals (crystal A and B) during growth. Upon the ice crystals making contact, the crystal planes show polycrystalline topography with a large density of grooves. From *Cascajo-Castresana et al.* [2021].

that has suggested these continuous melting transitions [*Dash*, 1999]. These deformations of the crystal facet likely affect the crystal's optical properties and the nature and size of the surface thereby influencing heterogeneous (gas-to-surface) processes.

Ice crystal shapes under typical atmospheric growth and sublimation conditions were studied by *Magee et al.* [2014] due to their relevance for ice crystal optical properties. ESEM allowed them to study in detail the mesoscopic roughness of ice crystals. Figure 20 shows the surface roughness of ice crystals under growing and sublimating conditions [*Magee et al.*, 2014]. Figure 20a displays distinct surface roughness on the basal facets and prism facets of the growing crystal. Microfaceting on basal and prism facets was also observed as shown in Fig. 20b although it was only observed during steady growth at temperatures below -35 °C. Ice crystal facets display very different surface roughness upon sublimation as evident from Fig. 20c and d. In this case, concave and scalloped depressions develop away from the original surface. Scalloping is often initiated at the site of roughness produced during previous growth. The sublimation process also seemed to occur outward from multiple centers, often at the site of a former ridge or ledge.

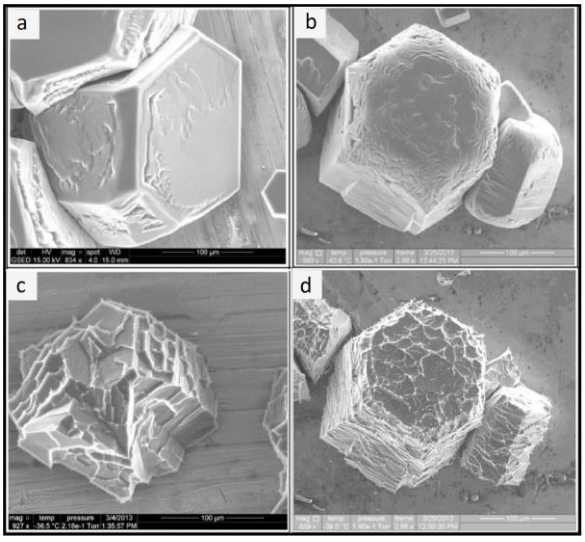

Figure 20. Environmental scanning electron microscopy (ESEM) images of mesoscopic surface topography of growing ice crystals (a and b) and sublimating ice crystals (c and d). Adapted from *Magee et al.* [2014].

In a follow-up study *Magee et al.* [2021] captured ice crystals in a cirrus cloud for ESEM/EDS analysis during the Ice Cryo-Encapsulation by Balloon (ICE-Ball) experiment. The balloon borne crystal catcher payload consists of cryo-vessels with sweep tubes that open to capture and store ice crystals in small, hermetically sealed cryo-encapsulation cells. Imaging of thousands of cirrus particles revealed diverse and unanticipated particle morphologies, ice crystal habit heterogeneity, and multiple scales of mesoscopic roughening.

Aerosol particles embedded in ice crystals were also observed [*Magee et al.*, 2021] as displayed in SEM images of ice crystals captured in cirrus clouds (Fig. 21). An ice crystal rosette is depicted in Fig. 21a. Contrary to the ice crystal habit diagram shown in Fig. 4, the collected ice crystals show much greater complexity with surface pits and mesoscopic surface roughening. Figure 21b shows various ice crystals to which aerosol particles visible as white small dots are

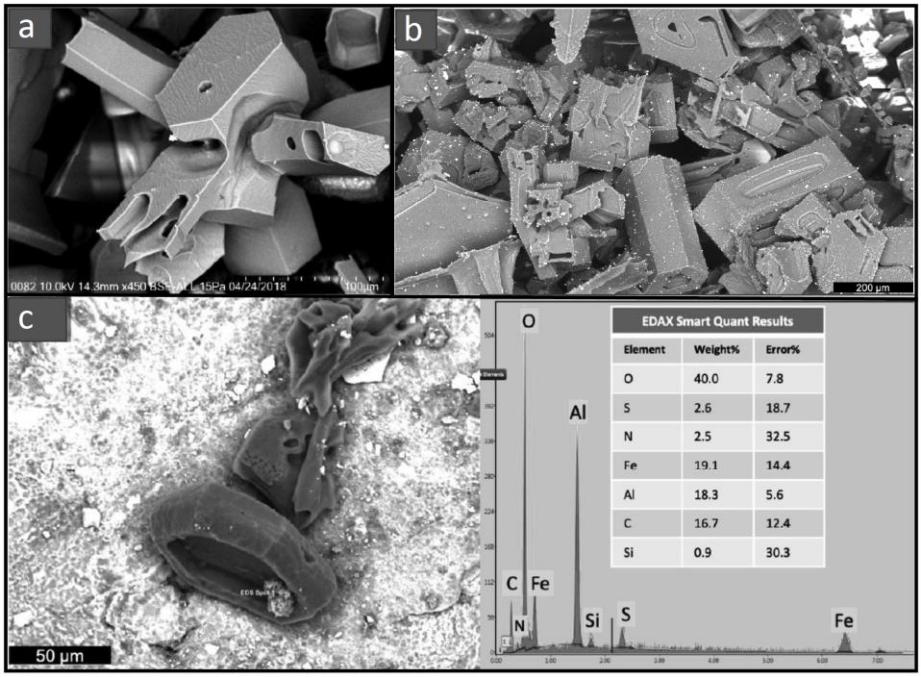

Figure 21. Captured cirrus ice crystals for cryo-scanning electron microscopy (cryo-SEM) and energy-dispersive X-ray spectroscopy (EDS). (a) A rosette with mixed-aspect crystals and several geometric surface pits and high mesoscopic roughening. (b) Ice crystals with embedded aerosol particles (white spots on crystal faces). (c) Shallow hollowed trigonal ice particle with iron-rich embedded aerosol. The EDS spectrum of the iron-rich aerosol is given on the right hand side of (c). Adapted from *Magee et al.* [2021].

attached. Lastly, an iron-rich aerosol particle (Fig. 21c) adhering in the shallow hollow of a trigonal single ice crystal was identified by means of EDS analysis.

Application of ESEM for ice crystal growth and sublimation studies clearly has generated detailed insights into the evolution of ice crystals and demonstrated that ice crystal habits on the microscale can be tremendously complex. Classical ice crystal habit diagrams, such as shown in Fig. 4, obtained typically with optical microscopy, do not capture the intricate nature of ice crystal facet surfaces that can include mesoscopic roughening, surface pits, strands, and grooves. All these features can influence ice crystal's optical properties and physical interaction and chemical reactivity with gas-phase species.

4 Experimental requirements and challenges

Microanalysis techniques to study ice nucleation and ice crystal growth have only gained traction in the last 15 years. Thus, this research area is expected to continue to evolve. This year's successful quantitative observation of ice nucleation in a STXM instrument is a clear indication of the advancement of microanalyses in studying atmospheric ice nucleation and ice crystal formation. In the this section, the sample requirements, radiation effects, and the role of standard INPs, are briefly summarized.

4.1 Sample preparation

When studying ice nucleation, sample supporting substrates suitable for the various microanalysis techniques must not interfere with the ice nucleation process. In other words, the supporting substrate should be more hydrophobic and less ice nucleation active compared to the particles or substrate being examined. This is specifically true when studying homogeneous ice nucleation which requires substrates that remain inert with regard to ice formation for

temperatures as low as ~235 K [*Knopf*, 2003; *Knopf and Lopez*, 2009; *Knopf and Rigg*, 2011]. When studying colder homogeneous freezing temperatures, a non-substrate approach is most suitable [*Amaya and Wyslouzil*, 2018; *Laksmono et al.*, 2015]. Water droplets-oil emulsions have been employed to study ice nucleation, allowing the observation of a large number of micrometer-sized droplets separated by oil [*Reicher et al.*, 2018; *Riechers et al.*, 2013; *Shardt et al.*, 2022; *Stan et al.*, 2009; *Tarn et al.*, 2021]. However, currently, this approach excludes the application of microanalysis techniques described here.

For Raman studies, typically hydrophobically coated glass or quartz slides are employed [*Knopf*, 2003; *Knopf et al.*, 2002; *Knopf et al.*, 2003]. Silicon nitride coated silicon wafer chips are suitable for studies of heterogeneous ice nucleation by deposited particles [*Knopf et al.*, 2022; *Lata et al.*, 2021; *Wang et al.*, 2016]. For STXM applications, silicon nitride-coated Si frames can be used for ice nucleation studies, although due to membrane thickness of only ~100 nm, sample handling is difficult and ensuring temperature homogeneity across the membrane, is challenging [*Alpert et al.*, 2022a; *Knopf et al.*, 2014].

4.2 Sample size for ice nucleation studies

The sample size affects the experimental procedure and results in various ways. The sensitivity of ice nucleation is determined by how many particles can be observed at the same time. For example, in a sample with 100000 deposited particles, observing one ice nucleation event, places the detection limit at 10^{-5}. This is a very low detection limit representing an inherent strength of the particle-on-substrate approach when studying ice nucleation. If freezing kinetics are to be determined, the greater the number of observed ice nucleation events, the smaller the uncertainty due to the stochastic nature of nucleation process [*Alpert and Knopf*, 2016; *Knopf et al.*, 2020;

Koop, 2004; *Koop et al.*, 1997; *Pruppacher and Klett*, 1997]. This requirement necessitates repetition of experiments to increase the number of observed ice nucleation events.

As discussed in the case of multimodal and in situ ice nucleation studies, typically the entire sample area is observed to determine which particle or at which location ice crystals formed initially. This allows for subsequent in detail examination and relocation of the particle or surface feature that initiated the ice nucleation. However, if the sample area is large, necessitating a large field of view, instrument resolution is usually low, thereby eliminating the main capability of the instrument. For this reason, a compromise in design of the sample stage and experimental procedure must be made to ensure that the entire temperature-controlled sample area can be visualized. The very first experiment should establish that ice indeed forms only on the sample stage on which the supporting substrate is mounted. As such the design of the cold stage must be the coldest area in the experimental setup. If ice forms outside the sample area, the humidity field above the sample can be distorted. The same holds true when a specific sample area is investigated for ice formation at greater magnification, but an ice crystal forms outside the field of view. In this case, the humidity above the visualized sample section may not be the one set for the observed conditions. In other words, as soon ice forms and the ice crystal grows, it depletes the water partial pressure resulting in pressure differences across the sample. At 1 atm and 253 K and a diffusion coefficient of water vapor of about 0.18 $cm^2\ s^{-1}$, the steady state concentration profile around a 10 µm particle establishes after 3.4×10^{-7} s [*Seinfeld and Pandis*, 1998]. This concentration profile will then govern the flux of water molecules towards the sink, here, the low-pressure or water vapor depleted region around the ice crystal. Hence, the adjustment of the concentration profile and subsequent transport of water molecules can be assumed to occur more rapidly than the detection of the resulting effects. Those include

evaporation of droplets or the necessity of significant increase in humidity to initiate the next ice nucleation event. For this reason, if the thermodynamic conditions under which ice nucleation proceeds are crucial measurement parameters, typically only the first ice nucleation event is considered in the analysis [*Alpert et al.*, 2022a; *Dymarska et al.*, 2006; *Knopf et al.*, 2014; *Wang and Knopf*, 2011; *Wang et al.*, 2016].

4.3 Beam induced radiation effects

The energy deposited onto the substrate or particle by the excitation source can impact the temperature of the particle and in the worst-case scenario result in compositional alterations. Significant warming of the sample can alter the sample's propensity to initiate ice nucleation. For example, at 253 K, a sample warming by 1 K, can alter S_{ice} by 10%. Hence, careful corroboration of sample warming upon radiation exposure has to be conducted for different beam energies before examining ice nucleation processes. This will also depend on the absorbing nature of the sample being examined.

Laser light as excitation source for Raman scattering can deposit energy, thus, heat onto a particle or substrate sample. This depends on the absorbing nature of the examined material. The radiation effect causing sample warming can be assessed by measuring melting points of organic liquids and ice for different laser power and exposure times [*Knopf et al.*, 2003]. Changes in spectral features, e.g., the surface area of a vibration band, for different laser exposure at constant temperature can also indicate potential heating and compositional changes of the sample.

When using ESEM to examine surface features serving as sites for ice nucleation and to determine nucleation kinetics, the electron beam can affect these measurements by its effect on water. The electron beam used in SEM application may induce dissociation of water molecules when studying water-substrate interactions [*Bjornehohn et al.*, 2016; *Hodgson and Haq*, 2009;

Pach and Verdaguer, 2022; *Tamtogl et al.*, 2021]. Higher beam energies needed to achieve greater resolution will consequently yield more water dissociation likely impacting the humidity field and the secondary electron emission and detection. Such radiation effects are the likely main reasons why resolution when studying ice nucleation can be limited. This phenomenon raises the question of whether an electron beam approach can be used to image the location of the critical ice nucleus at nano- and subnano-scales to resolve the physicochemical nature of an INAS.

AFM might provide an alternative method to study atmospheric ice nucleation and ice crystal growth in the future [*Thürmer and Nie*, 2013]. This method does not suffer from beam radiation effects. Recent developments demonstrate the capability of AFM to monitor the growth of 2D ice layers [*Ma et al.*, 2020] and multilayer ice [*Peng et al.*, 2022]. These studies apply non-contact AFM and qPlus-AFM that uses functionalized tips that allow direct imaging of the chemical structure of molecules with single bond resolution [*Peng et al.*, 2022]. Furthermore, *Chasnitsky et al*. [2023] developed a new AFM setup that allows to image ice crystal surfaces in supercooled water containing antifreeze agents at the sub-10 nm scale. Successful application of AFM to ice nucleation and growth will depend on cantilever tip design, operating mode, and low noise sensors [*Peng et al.*, 2022].

4.4 Standard ice-nucleating particles

INPs with defined ice nucleation properties and exactly determined surface area would greatly benefit ice nucleation research by allowing assessment of our predictive understanding of ice nucleation and evaluation of ice nucleation instrument performance. Two ice nucleation measurement intercomparison studies that included up to 17 different instruments have been conducted in recent years [*DeMott et al.*, 2018; *Hiranuma et al.*, 2015]. Illite NX and potassium

feldspar mineral dusts, two natural soil dusts, and bacterial matter served as test INPs to assess the performance of the various instrumentation. In the case of illite INPs, differences in INAS density of about three orders of magnitude among the instruments were observed [*Hiranuma et al.*, 2015]. As one of the many outcomes of the intercomparison study described by *DeMott et al.* [2018] was the requirement of knowing the accurate size of INPs being probed by the instruments. Clearly, even when employing commercially available particles derived from natural resources (like minerals), on a nanoscale resolution the particles will likely not exactly resemble each other, leading to further uncertainties in the evaluation of ice nucleation instrumentation and our understanding of ice nucleation processes.

Artificially generated standard surfaces and particles with well-controlled nanoscale physicochemical properties will allow the systematic study of ice nucleation. Microanalysis techniques will play a crucial role in characterizing the chemical nature of such standard surfaces and for determining the surface area accurately. Ice-nucleating substrate surfaces where specific chemical or morphological features are located within nanoscale resolution will provide the means to evaluate the fundamental processes of ice nucleation [*Knopf et al.*, 2020]. This approach has currently only been attempted in molecular dynamics simulations [*Cabriolu and Li*, 2015; *Cox et al.*, 2015; *Croteau et al.*, 2010; *Lupi et al.*, 2014; *Qiu et al.*, 2017; *Sosso et al.*, 2016; *Zielke et al.*, 2016]. Design of artificial substrates will allow the region where ice nucleation commences to be confined, thereby decreasing the necessary field of view and increasing the observational resolution. This should facilitate optimization of the microanalytical detection method.

Assuming the existence of a standard INP that has an accurately defined ice nucleation efficiency and exactly known surface area, how would immersion freezing results look like when

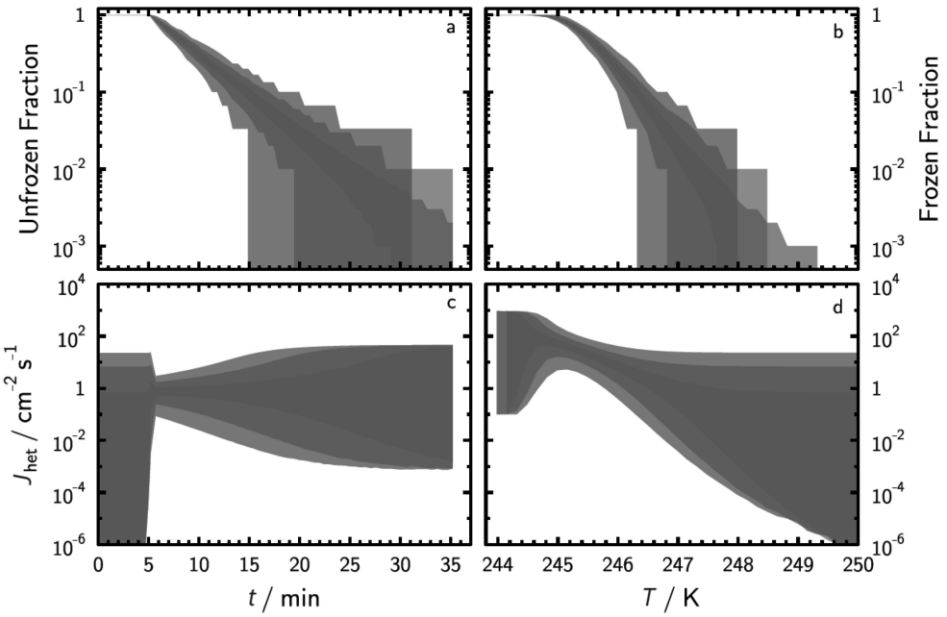

Figure 22. Application of standard INPs that have exactly the same surface area and ice nucleation efficiency in immersion freezing simulations using 30, 100, and 1000 observed freezing events of droplets depicted as light, intermediate, and dark grey colors, respectively. Isothermal and constant cooling rate freezing experiments are depicted in (a) and (c) and (b) and (d), respectively. Sensitivity of uncertainties in unfrozen fraction, frozen fraction, and heterogeneous ice nucleation rate coefficients, J_{het}, are displayed. The shading in unfrozen and frozen fraction curves in (a) and (b), respectively, represent 5th and 95th percentiles. The shadings in (c) and (d) represent the upper and lower fiducial limits of the derived J_{het} values. From *Knopf et al.* [2020].

employing these INPs? Application of a Monte Carlo method of 10^5 freezing simulations, *Knopf et al.* [2020] discuss the expected results of isothermal and constant cooling rate immersion freezing experiments when using INPs with perfectly the same surface area. Figure 22 shows these sensitivity results for isothermal, where the temperature is held constant, and constant cooling rate, where the sample of droplets are cooled at a constant rate, experiments using droplets that contain one INP with the same surface area. As time passes or the droplet sample is cooled, more and more of the initial liquid droplets freeze, thereby changing the unfrozen (UNF) and frozen fraction (FF) of droplets in the sample. Since the UNF and FF are exponential functions of J_{het}, a log-linear dependency of UNF with time is expected for isothermal freezing experiments and a sigmoidal curve for FF is expected for constant cooling rate experiments (Fig. 22a and b) [*Knopf et al.*, 2020; *Pruppacher and Klett*, 1997]. It is evident that a smaller number

of observed ice nucleation events results in a larger uncertainty of UNF and FF. Hence, the stochastic nature of ice nucleation would still impose significant uncertainties, i.e., data scatter, in the experimental results. Thus, even with a standard INP at hand, a sufficiently large number of freezing events have to be observed to minimize uncertainties. Figure 22c and d show the corresponding J_{het} values for isothermal and constant cooling rate experiments, respectively. The derived J_{het} values represent constant J_{het} values for isothermal freezing experiments and a log-linear dependency of J_{het} on temperature for the constant cooling rate experiments. The greater the number of observed freezing events, the smaller the uncertainty in J_{het}. Since statistically, most of the droplets freeze around the median of the UNF or FF the corresponding uncertainties are lowest at that point. Whereas the few freezing events that occur at shortest and longest times or warmest and coldest temperatures yield greatest uncertainties. Hence, even when applying INPs with perfectly controlled and characterized surface area, some scatter in the freezing data can be expected if immersion freezing follows CNT. Hence, standard INPs will allow for careful evaluation of the application of CNT or INAS based parameterizations and determine their scalability to atmospheric processes.

Acknowledgements. This study was supported by the Atmospheric System Research Program of the U.S. Department of Energy (DOE), Office of Science, Office of Biological and Environmental Research (OBER), Climate and Environmental Sciences Division (CESD). DAK acknowledges support by the U.S. DOE grant DE-SC0021034. DAK is indebted to Josephine Aller and Peter Alpert for proofreading this manuscript.

Data Availability Statement. All data and methods discussed in this book chapter

have been published previously as given in the references. All data and methods needed to draw the conclusions presented in this chapter are shown in this chapter.

References

Alpert, P. A., J. Y. Aller, and D. A. Knopf (2011), Initiation of the ice phase by marine biogenic surfaces in supersaturated gas and supercooled aqueous phases, *Phys. Chem. Chem. Phys.*, *13*(44), 19882-19894.

Alpert, P. A., A. Boucly, S. Yang, H. Yang, K. Kilchhofer, Z. Luo, C. Padeste, S. Finizio, M. Ammann, and B. Watts (2022a), Ice nucleation imaged with X-ray spectro-microscopy, *Environ. sci. Atmos.*, doi:10.1039/d1ea00077b.

Alpert, P. A., W. P. Kilthau, R. E. O'Brien, R. C. Moffet, M. K. Gilles, B. Wang, A. Laskin, J. Y. Aller, and D. A. Knopf (2022b), Ice-nucleating agents in sea spray aerosol identified and quantified with a holistic multi-modal freezing model, *Sci. Adv.*, *8*(44), eabq6842, doi:10.1126/sciadv.abq6842.

Alpert, P. A., and D. A. Knopf (2016), Analysis of isothermal and cooling-rate-dependent immersion freezing by a unifying stochastic ice nucleation model, *Atmos. Chem. Phys.*, *16*(4), 2083-2107, doi:10.5194/acp-16-2083-2016.

Amaya, A. J., and B. E. Wyslouzil (2018), Ice nucleation rates near similar to 225 K, *J. Chem. Phys.*, *148*(8), 9, doi:10.1063/1.5019362.

Ansmann, A., H. Baars, M. Tesche, D. Mueller, D. Althausen, R. Engelmann, T. Pauliquevis, and P. Artaxo (2009), Dust and smoke transport from Africa to South America: Lidar profiling over Cape Verde and the Amazon rainforest, *Geophys. Res. Lett.*, *36*, L11802, doi:10.1029/2009gl037923.

Bacon, N. J., and B. D. Swanson (2000), Laboratory measurements of light scattering by single levitated ice crystals, *J. Atmos. Sci.*, *57*(13), 2094-2104.

Bailey, M., and J. Hallett (2002), Nucleation effects on the habit of vapour grown ice crystals from -18 to -42 degrees C, *Q. J. R. Meteorol. Soc.*, *128*(583), 1461-1483, doi:10.1002/qj.200212858304.

Bailey, M., and J. Hallett (2004), Growth rates and habits of ice crystals between -20 degrees and -70 degrees C, *J. Atmos. Sci.*, *61*(5), 514-544.

Bailey, M. P., and J. Hallett (2009), A Comprehensive Habit Diagram for Atmospheric Ice Crystals: Confirmation from the Laboratory, AIRS II, and Other Field Studies, *J. Atmos. Sci.*, *66*(9), 2888-2899, doi:10.1175/2009jas2883.1.

Bailo, E., and V. Deckert (2008), Tip-enhanced Raman scattering, *Chem. Soc. Rev.*, *37*(5), 921-930, doi:10.1039/b705967c.

Baker, A., and T. Peter (2008), Small-scale cloud processes and climate, *Nat. Geosci.*, *451*(17), 299-300.

Baker, M. B. (1997), Cloud microphysics and climate, *Science*, *276*(5315), 1072-1078.

Baustian, K. J., D. J. Cziczo, M. E. Wise, K. A. Pratt, G. Kulkarni, A. G. Hallar, and M. A. Tolbert (2012), Importance of aerosol composition, mixing state, and morphology for heterogeneous ice nucleation: A combined field and laboratory approach, *J. Geophys. Res.*, *117*, D06217, doi:10.1029/2011jd016784.

Baustian, K. J., M. E. Wise, E. J. Jensen, G. P. Schill, M. A. Freedman, and M. A. Tolbert (2013), State transformations and ice nucleation in amorphous (semi-)solid organic aerosol, *Atmos. Chem. Phys.*, *13*(11), 5615-5628, doi:10.5194/acp-13-5615-2013.

Baustian, K. J., M. E. Wise, and M. A. Tolbert (2010), Depositional ice nucleation on solid ammonium sulfate and glutaric acid particles, *Atmos. Chem. Phys.*, *10*, 2307-2317.

Bentley, W. A., and W. J. Humphreys (1931), *Snow Crystals*, 226 pp., McGraw-Hill, New York, London.

Berkemeier, T., M. Shiraiwa, U. Pöschl, and T. Koop (2014), Competition between water uptake and ice nucleation by glassy organic aerosol particles, *Atmos. Chem. Phys.*, *14*(22), 12513-12531, doi:10.5194/acp-14-12513-2014.

Bertram, A. K., T. Koop, L. T. Molina, and M. J. Molina (2000), Ice formation in (NH4)(2)SO4-H2O particles, *J. Phys. Chem. A*, *104*(3), 584-588.

Bjornehohn, E., et al. (2016), Water at Interfaces, *Chem. Rev.*, *116*(13), 7698-7726, doi:10.1021/acs.chemrev.6b00045.

Bogdan, A. (2018), Ice Clouds: Atmospheric Ice Nucleation Concept versus the Physical Chemistry of Freezing Atmospheric Drops, *J. Phys. Chem. A*, *122*(39), 7777-7781, doi:10.1021/acs.jpca.8b07926.

Bogdan, A., and M. J. Molina (2017), Physical Chemistry of the Freezing Process of Atmospheric Aqueous Drops, *J. Phys. Chem. A*, *121*(16), 3109-3116, doi:10.1021/acs.jpca.7b02571.

Bogdan, A., M. J. Molina, and H. Tenhu (2016), Freezing and glass transitions upon cooling and warming and ice/freeze-concentration-solution morphology of emulsified aqueous citric acid, *Eur. J. Pharm. Biopharm.*, *109*, 49-60, doi:10.1016/j.ejpb.2016.09.012.

Boucher, O., et al. (2013), Clouds and Aerosols, in *Climate Change 2013: The Physical Science Basis. Contribution of Working Group I to the Fifth Assessment Report of the Intergovernmental Panel on Climate Change*, edited by T. F. Stocker, D. Qin, G.-K. Plattner, M. Tignor, S. K. Allen, J. Boschung, A. Nauels, Y. Xia, V. Bex and P. M. Midgley, Cambridge University Press, Cambridge, United Kingdom and New York, NY, USA.

Cabriolu, R., and T. S. Li (2015), Ice nucleation on carbon surface supports the classical theory for heterogeneous nucleation, *Phys. Rev. E*, *91*(5), 052402, doi:10.1103/PhysRevE.91.052402.

Campion, A., and P. Kambhampati (1998), Surface-enhanced Raman scattering, *Chem. Soc. Rev.*, *27*(4), 241-250, doi:10.1039/a827241z.

Cascajo-Castresana, M., S. Morin, and A. M. Bittner (2021), The ice-vapour interface during growth and sublimation, *Atmos. Chem. Phys.*, *21*(24), 18629-18640, doi:10.5194/acp-21-18629-2021.

Charnawskas, J. C., et al. (2017), Condensed-phase biogenic-anthropogenic interactions with implications for cold cloud formation, *Faraday Discuss.*, *200*, 164-195, doi:10.1039/C7FD00010C.

Chasnitsky, M., S. R. Cohen, Y. Rudich, and I. Braslavsky (2023), Atomic force microscopy imaging of ice crystal surfaces formed in aqueous solutions containing ice-binding proteins, *J. Cryst. Growth*, *601*, 126961, doi:10.1016/j.jcrysgro.2022.126961.

Chen, X., J. P. Shu, and Q. Chen (2017), Abnormal gas-liquid-solid phase transition behaviour of water observed with in situ environmental SEM, *Sci Rep*, *7*, 10, doi:10.1038/srep46680.

Chen, Y. L., S. M. Kreidenweis, L. M. McInnes, D. C. Rogers, and P. J. DeMott (1998), Single particle analyses of ice nucleating aerosols in the upper troposphere and lower stratosphere, *Geophys. Res. Lett.*, *25*(9), 1391-1394.

China, S., et al. (2017), Ice cloud formation potential by free tropospheric particles from long-range transport over the Northern Atlantic Ocean, *J. Geophys. Res.*, *122*(5), 3065-3079, doi:10.1002/2016jd025817.

Cialla, D., A. Marz, R. Bohme, F. Theil, K. Weber, M. Schmitt, and J. Popp (2012), Surface-enhanced Raman spectroscopy (SERS): progress and trends, *Anal. Bioanal. Chem.*, *403*(1), 27-54, doi:10.1007/s00216-011-5631-x.

Coluzza, I., et al. (2017), Perspectives on the Future of Ice Nucleation Research: Research Needs and Unanswered Questions Identified from Two International Workshops, *Atmosphere*, *8*(8), doi:10.3390/atmos8080138.

Connolly, P. J., O. Möhler, P. R. Field, H. Saathoff, R. Burgess, T. Choularton, and M. Gallagher (2009), Studies of heterogeneous freezing by three different desert dust samples, *Atmos. Chem. Phys.*, *9*(8), 2805-2824, doi:10.5194/acp-9-2805-2009.

Cox, S. J., S. M. Kathmann, B. Slater, and A. Michaelides (2015), Molecular simulations of heterogeneous ice nucleation. I. Controlling ice nucleation through surface hydrophilicity, *J. Chem. Phys.*, *142*(18), 184704, doi:10.1063/1.4919714.

Croteau, T., A. K. Bertram, and G. N. Patey (2010), Water Adsorption on Kaolinite Surfaces Containing Trenches, *J. Phys. Chem. A*, *114*(5), 2171-2178, doi:10.1021/jp910045u.

Cziczo, D. J., K. D. Froyd, C. Hoose, E. J. Jensen, M. H. Diao, M. A. Zondlo, J. B. Smith, C. H. Twohy, and D. M. Murphy (2013), Clarifying the Dominant Sources and Mechanisms of Cirrus Cloud Formation, *Science*, *340*(6138), 1320-1324, doi:10.1126/science.1234145.

Cziczo, D. J., L. A. Ladino, Y. Boose, Z. A. Kanji, P. Kupiszewski, S. Lance, S. Mertes, and H. Wex (2017), Measurements of Ice Nucleating Particles and Ice Residuals, in *Ice Formation and Evolution in Clouds and Precipitation: Measurement and Modeling Challenges*, edited, pp. 8.1-8.13, American Meteorological Society, doi:10.1175/AMSMONOGRAPHS-D-16-0008.1.

Cziczo, D. J., D. M. Murphy, P. K. Hudson, and D. S. Thomson (2004), Single particle measurements of the chemical composition of cirrus ice residue during CRYSTAL-FACE, *J. Geophys. Res.*, *109*(D4), D04201, doi:10.1029/2003JD004032.

Dash, J. G. (1999), History of the search for continuous melting, *Rev. Mod. Phys.*, *71*(5), 1737-1743, doi:10.1103/RevModPhys.71.1737.

Dash, J. G., A. W. Rempel, and J. S. Wettlaufer (2006), The physics of premelted ice and its geophysical consequences, *Rev. Mod. Phys.*, *78*(3), 695-741, doi:10.1103/RevModPhys.78.695.

David, R. O., C. Marcolli, J. Fahrni, Y. Qiu, Y. A. Perez Sirkin, V. Molinero, F. Mahrt, D. Brühwiler, U. Lohmann, and Z. A. Kanji (2019), Pore condensation and freezing is responsible for ice formation below water saturation for porous particles, doi:10.1073/pnas.1813647116.

de Boer, G., H. Morrison, M. D. Shupe, and R. Hildner (2011), Evidence of liquid dependent ice nucleation in high-latitude stratiform clouds from surface remote sensors, *Geophys. Res. Lett.*, *38*, L01803, doi:10.1029/2010gl046016.

DeMott, P. J. (2002), Laboratory Studies of Cirrus Cloud Processes, in *Cirrus*, edited by D. K. Lynch, K. Sassen, D. O. Starr and G. Stephens, pp. 102-136, Oxford University Press, New York.

DeMott, P. J., et al. (2018), The Fifth International Workshop on Ice Nucleation phase 2 (FIN-02): laboratory intercomparison of ice nucleation measurements *Atmos. Meas. Tech.*, *11*, doi:10.5194/amt-11-6231-2018.

DeMott, P. J., A. J. Prenni, X. Liu, S. M. Kreidenweis, M. D. Petters, C. H. Twohy, M. S. Richardson, T. Eidhammer, and D. C. Rogers (2010), Predicting global atmospheric ice nuclei distributions and their impacts on climate, *Proc. Natl. Acad. Sci. U. S. A.*, *107*(25), 11217-11222, doi:10.1073/pnas.0910818107.

Durant, A. J., and R. A. Shaw (2005), Evaporation freezing by contact nucleation inside-out, *Geophys. Res. Lett.*, *32*(20), L20814, doi:10.1029/2005gl024175.

Dymarska, M., B. J. Murray, L. M. Sun, M. L. Eastwood, D. A. Knopf, and A. K. Bertram (2006), Deposition ice nucleation on soot at temperatures relevant for the lower troposphere, *J. Geophys. Res.*, *111*(D4), D04204, doi:Doi 10.1029/2005jd006627.

Field, P. R., et al. (2017), Secondary Ice Production: Current State of the Science and Recommendations for the Future, in *Ice Formation and Evolution in Clouds and Precipitation: Measurement and Modeling Challenges*, edited, pp. 7.1-7.20, American Meteorological Society, doi:10.1175/AMSMONOGRAPHS-D-16-0014.1.

Fletcher, N. H. (1958), Size Effect in Heterogeneous Nucleation, *J. Chem. Phys.*, *29*(3), 572-576.

Friddle, R. W., and K. Thürmer (2019), How nanoscale surface steps promote ice growth on feldspar: microscopy observation of morphology-enhanced condensation and freezing, *Nanoscale*, *11*(44), 21147-21154, doi:10.1039/c9nr08729j.

Friddle, R. W., and K. Thürmer (2020), Mapping ice formation to mineral-surface topography using a micro mixing chamber with video and atomic-force microscopy, *Atmos. Meas. Tech.*, *13*(5), 2209-2218, doi:10.5194/amt-13-2209-2020.

Hartmann, D. L. (2016), Tropical anvil clouds and climate sensitivity, *Proc. Natl. Acad. Sci. U. S. A.*, *113*(32), 8897-8899, doi:10.1073/pnas.1610455113.

Hegg, D. A., and M. B. Baker (2009), Nucleation in the atmosphere, *Rep. Prog. Phys.*, *72*(5), 056801, doi:10.1088/0034-4885/72/5/056801.

Heintzenberg, J., K. Okada, and J. Strom (1996), On the composition of non-volatile material in upper tropospheric aerosols and cirrus crystals, *Atmos. Res.*, *41*(1), 81-88, doi:10.1016/0169-8095(95)00042-9.

Held, I. M., and B. J. Soden (2000), Water vapor feedback and global warming, *Annu. Rev. Energ. Env.*, *25*, 441-475.

Heymsfield, A. J., et al. (2017), Cirrus Clouds, *Meteorological Monographs*, *58*, 2.1-2.26, doi:10.1175/amsmonographs-d-16-0010.1.

Hiranuma, N., et al. (2015), A comprehensive laboratory study on the immersion freezing behavior of illite NX particles: a comparison of 17 ice nucleation measurement techniques, *Atmos. Chem. Phys.*, *15*(5), 2489-2518, doi:10.5194/acp-15-2489-2015.

Hiranuma, N., S. D. Brooks, R. C. Moffet, A. Glen, A. Laskin, M. K. Gilles, P. Liu, A. M. Macdonald, J. W. Strapp, and G. M. McFarquhar (2013), Chemical characterization of individual particles and residuals of cloud droplets and ice crystals collected on board research aircraft in the ISDAC 2008 study, *J. Geophys. Res.*, *118*(12), 6564-6579, doi:10.1002/jgrd.50484.

Hodgson, A., and S. Haq (2009), Water adsorption and the wetting of metal surfaces, *Surf. Sci. Rep.*, *64*(9), 381-451, doi:10.1016/j.surfrep.2009.07.001.

Holden, M. A., T. F. Whale, M. D. Tarn, D. O'Sullivan, R. D. Walshaw, B. J. Murray, F. C. Meldrum, and H. K. Christenson (2019), High-speed imaging of ice nucleation in water proves the existence of active sites, *Sci. Adv.*, *5*(2), 10, doi:10.1126/sciadv.aav4316.

Hoose, C., and O. Möhler (2012), Heterogeneous ice nucleation on atmospheric aerosols: a review of results from laboratory experiments, *Atmos. Chem. Phys.*, *12*(20), 9817-9854, doi:10.5194/acp-12-9817-2012.

Jensen, E. J., et al. (2009), On the importance of small ice crystals in tropical anvil cirrus, *Atmos. Chem. Phys.*, *9*(15), 5519-5537.

Kanji, Z. A., L. A. Ladino, H. Wex, Y. Boose, M. Burkert-Kohn, D. J. Cziczo, and M. Krämer (2017), Overview of Ice Nucleating Particles, in *Ice Formation and Evolution in Clouds and Precipitation: Measurement and Modeling Challenges*, edited, pp. 1.1-1.33, American Meteorological Society, doi:DOI: 10.1175/AMSMONOGRAPHS-D-16-0006.1.

Kiselev, A., F. Bachmann, P. Pedevilla, S. J. Cox, A. Michaelides, D. Gerthsen, and T. Leisner (2017), Active sites in heterogeneous ice nucleation—the example of K-rich feldspars, *Science*, *355*(6323), 367-371, doi:10.1126/science.aai8034.

Knopf, D. A. (2003), Thermodynamic Properties and Nucleation Processes of Upper Tropospheric and Lower Stratospheric Aerosol Particles, Ph.D. thesis, 163 pp, Swiss Federal Institute of Technology, Zurich.

Knopf, D. A., P. A. Alpert, and B. Wang (2018), The Role of Organic Aerosol in Atmospheric Ice Nucleation: A Review, *ACS Earth Space Chem.*, *2*(3), 168–202, doi:10.1021/acsearthspacechem.7b00120.

Knopf, D. A., P. A. Alpert, B. Wang, R. E. O'Brien, S. T. Kelly, A. Laskin, M. K. Gilles, and R. C. Moffet (2014), Microspectroscopic imaging and characterization of individually identified ice nucleating particles from a case field study, *J. Geophys. Res.*, *119*, 10365-10381, doi:10.1002/2014JD021866.

Knopf, D. A., P. A. Alpert, A. Zipori, N. Reicher, and Y. Rudich (2020), Stochastic nucleation processes and substrate abundance explain time-dependent freezing in supercooled droplets, *npj Clim. Atmos. Sci.*, *3*(2), 1-9, doi:10.1038/s41612-020-0106-4.

Knopf, D. A., et al. (2021), Aerosol–Ice Formation Closure: A Southern Great Plains Field Campaign, *B. Am. Meteorol. Soc.*, *102*(10), E1952–E1971 doi:10.1175/BAMS-D-20-0151.1.

Knopf, D. A., et al. (2022), Micro-spectroscopic and freezing characterization of ice-nucleating particles collected in the marine boundary layer in the eastern North Atlantic, *Atmos. Chem. Phys.*, *22*(8), 5377-5398, doi:10.5194/acp-22-5377-2022.

Knopf, D. A., and T. Koop (2006), Heterogeneous nucleation of ice on surrogates of mineral dust, *J. Geophys. Res.*, *111*(D12), D12201, doi:10.1029/2005jd006894.

Knopf, D. A., T. Koop, B. P. Luo, U. G. Weers, and T. Peter (2002), Homogeneous nucleation of NAD and NAT in liquid stratospheric aerosols: insufficient to explain denitrification, *Atmos. Chem. Phys.*, *2*, 207-214.

Knopf, D. A., and M. D. Lopez (2009), Homogeneous ice freezing temperatures and ice nucleation rates of aqueous ammonium sulfate and aqueous levoglucosan particles for relevant atmospheric conditions, *Phys. Chem. Chem. Phys.*, *11*(36), 8056-8068, doi:Doi 10.1039/B903750k.

Knopf, D. A., B. P. Luo, U. K. Krieger, and T. Koop (2003), Thermodynamic dissociation constant of the bisulfate ion from Raman and ion interaction modeling studies of aqueous sulfuric acid at low temperatures, *J. Phys. Chem. A, 107*(21), 4322-4332.

Knopf, D. A., and Y. J. Rigg (2011), Homogeneous Ice Nucleation From Aqueous Inorganic/Organic Particles Representative of Biomass Burning: Water Activity, Freezing Temperatures, Nucleation Rates, *J. Phys. Chem. A, 115*(5), 762-773, doi:10.1021/jp109171g.

Knopf, D. A., B. Wang, A. Laskin, R. C. Moffet, and M. K. Gilles (2010), Heterogeneous nucleation of ice on anthropogenic organic particles collected in Mexico City, *Geophys. Res. Lett., 37*, L11803, doi:10.1029/2010GL043362.

Koop, T. (2004), Homogeneous ice nucleation in water and aqueous solutions, *Z. Phys. Chemie-Int. J. Res. Phys. Chem. Chem. Phys., 218*(11), 1231-1258.

Koop, T., J. Bookhold, M. Shiraiwa, and U. Pöschl (2011), Glass transition and phase state of organic compounds: dependency on molecular properties and implications for secondary organic aerosols in the atmosphere, *Phys. Chem. Chem. Phys., 13*(43), 19238-19255, doi:10.1039/c1cp22617g.

Koop, T., B. P. Luo, U. M. Biermann, P. J. Crutzen, and T. Peter (1997), Freezing of HNO3/H2SO4/H2O solutions at stratospheric temperatures: Nucleation statistics and experiments, *J. Phys. Chem. A, 101*(6), 1117-1133.

Koop, T., B. P. Luo, A. Tsias, and T. Peter (2000), Water activity as the determinant for homogeneous ice nucleation in aqueous solutions, *Nature, 406*(6796), 611-614, doi:10.1038/35020537.

Koop, T., H. P. Ng, L. T. Molina, and M. J. Molina (1998), A new optical technique to study aerosol phase transitions: The nucleation of ice from H2SO4 aerosols, *J. Phys. Chem. A, 102*(45), 8924-8931.

Korolev, A., and T. Leisner (2020), Review of experimental studies of secondary ice production, *Atmos. Chem. Phys., 20*(20), 11767-11797, doi:10.5194/acp-20-11767-2020.

Kreidenweis, S. M., Y. Chen, D. C. Rogers, and P. J. DeMott (1998), Isolating and identifying atmospheric ice-nucleating aerosols: a new technique, *Atmos. Res., 46*(3-4), 263-278.

Ladino Moreno, L. A., O. Stetzer, and U. Lohmann (2013), Contact freezing: a review of experimental studies, *Atmos. Chem. Phys., 13*(19), 9745-9769, doi:10.5194/acp-13-9745-2013.

Laksmono, H., et al. (2015), Anomalous Behavior of the Homogeneous Ice Nucleation Rate in "No-Man's Land", *J. Phys. Chem. Lett., 6*(14), 2826-2832, doi:10.1021/acs.jpclett.5b01164.

Laskin, A., M. K. Gilles, D. A. Knopf, B. Wang, and S. China (2016), Progress in the Analysis of Complex Atmospheric Particles, *Annu. Rev. Anal. Chem., 9*(1), 117-143, doi:10.1146/annurev-anchem-071015-041521.

Laskin, A., R. C. Moffet, and M. K. Gilles (2019), Chemical Imaging of Atmospheric Particles, *Accounts Chem. Res., 52*(12), 3419-3431, doi:10.1021/acs.accounts.9b00396.

Lata, N. N., B. Zhang, S. Schum, L. Mazzoleni, R. Brimberry, M. A. Marcus, W. H. Cantrell, P. Fialho, C. Mazzoleni, and S. China (2021), Aerosol Composition, Mixing State, and Phase State of Free Tropospheric Particles and Their Role in Ice Cloud Formation, *ACS Earth Space Chem., 5*(12), 3499-3510, doi:10.1021/acsearthspacechem.1c00315.

Lau, K. M., and H. T. Wu (2003), Warm rain processes over tropical oceans and climate implications, *Geophys. Res. Lett., 30*(24), 2290, doi:10.1029/2003gl018567.

Lawson, R. P., et al. (2019), A Review of Ice Particle Shapes in Cirrus formed In Situ and in Anvils, *J. Geophys. Res.*, *124*(17-18), 10049-10090, doi:10.1029/2018jd030122.

Libbrecht, K. G. (2005), The physics of snow crystals, *Rep. Prog. Phys.*, *68*(4), 855-895, doi:10.1088/0034-4885/68/4/r03.

Lohmann, U., and J. Feichter (2005), Global indirect aerosol effects: a review, *Atmos. Chem. Phys.*, *5*, 715-737.

Lohmann, U., E. Roeckner, W. D. Collins, A. J. Heymsfield, G. M. McFarquhar, and T. P. Barnett (1995), The role of water vapor and convection during the Central Equatorial Pacific Experiment from observations and model simulations, *J. Geophys. Res.*, *100*(D12), 26229-26245.

Lupi, L., A. Hudait, and V. Molinero (2014), Heterogeneous Nucleation of Ice on Carbon Surfaces, *J. Am. Chem. Soc.*, *136*(8), 3156-3164, doi:10.1021/ja411507a.

Ma, R. Z., et al. (2020), Atomic imaging of the edge structure and growth of a two-dimensional hexagonal ice, *Nature*, *577*(7788), 60-+, doi:10.1038/s41586-019-1853-4.

Mael, L. E., H. Busse, and V. H. Grassian (2019), Measurements of Immersion Freezing and Heterogeneous Chemistry of Atmospherically Relevant Single Particles with Micro-Raman Spectroscopy, *Anal. Chem.*, *91*(17), 11138-11145, doi:10.1021/acs.analchem.9b01819.

Magee, N., et al. (2021), Captured cirrus ice particles in high definition, *Atmos. Chem. Phys.*, *21*(9), 7171-7185, doi:10.5194/acp-21-7171-2021.

Magee, N. B., A. Miller, M. Amaral, and A. Cumiskey (2014), Mesoscopic surface roughness of ice crystals pervasive across a wide range of ice crystal conditions, *Atmos. Chem. Phys.*, *14*(22), 12357-12371, doi:10.5194/acp-14-12357-2014.

Marcolli, C. (2014), Deposition nucleation viewed as homogeneous or immersion freezing in pores and cavities, *Atmos. Chem. Phys.*, *14*(4), 2071-2104, doi:10.5194/acp-14-2071-2014.

Marcolli, C. (2020), Technical note: Fundamental aspects of ice nucleation via pore condensation and freezing including Laplace pressure and growth into macroscopic ice, *Atmos. Chem. Phys.*, *20*(5), 3209-3230, doi:10.5194/acp-20-3209-2020.

Martin, S. (2000), Phase transitions of aqueous atmospheric particles, *Chem. Rev.*, *100*, 3403-3453.

McFarquhar, G. M., P. Yang, A. Macke, and A. J. Baran (2002), A new parameterization of single scattering solar radiative properties for tropical anvils using observed ice crystal size and shape distributions, *J. Atmos. Sci.*, *59*(16), 2458-2478, doi:10.1175/1520-0469(2002)059<2458:Anposs>2.0.Co;2.

Mishchenko, M. I., W. B. Rossow, A. Macke, and A. A. Lacis (1996), Sensitivity of cirrus cloud albedo, bidirectional reflectance and optical thickness retrieval accuracy to ice particle shape, *J. Geophys. Res.-Atmos.*, *101*(D12), 16973-16985, doi:10.1029/96jd01155.

Mülmenstädt, J., O. Sourdeval, J. Delanoe, and J. Quaas (2015), Frequency of occurrence of rain from liquid-, mixed-, and ice-phase clouds derived from A-Train satellite retrievals, *Geophys. Res. Lett.*, *42*(15), 6502-6509, doi:10.1002/2015gl064604.

Murray, B. J., D. O'Sullivan, J. D. Atkinson, and M. E. Webb (2012), Ice nucleation by particles immersed in supercooled cloud droplets, *Chem. Soc. Rev.*, *41*(19), 6519-6554, doi:10.1039/C2CS35200A.

Nair, M., A. Husmann, R. E. Cameron, and S. M. Best (2018), In situ ESEM imaging of the vapor-pressure-dependent sublimation-induced morphology of ice, *Phys. Rev. Mater.*, *2*(4), 7, doi:10.1103/PhysRevMaterials.2.040401.

Nakaya, U. (1954), *Snow Crystals, Natural and Artificial*, 510 pp., Harvard University Press, Cambridge.

Pach, E., and A. Verdaguer (2022), Studying Ice with Environmental Scanning Electron Microscopy, *Molecules*, *27*(1), 17, doi:10.3390/molecules27010258.

Pedersen, C., A. Mihranyan, and M. Stromme (2011), Surface Transition on Ice Induced by the Formation of a Grain Boundary, *Plos One*, *6*(9), 4, doi:10.1371/journal.pone.0024373.

Peng, J. B., J. Guo, R. Z. Ma, and Y. Jiang (2022), Water-solid interfaces probed by high-resolution atomic force microscopy, *Surf. Sci. Rep.*, *77*(1), doi:10.1016/j.surfrep.2021.100549.

Petzold, A., J. Strom, S. Ohlsson, and F. P. Schroder (1998), Elemental composition and morphology of ice-crystal residual particles in cirrus clouds and contrails, *Atmos. Res.*, *49*(1), 21-34, doi:10.1016/s0169-8095(97)00083-5.

Pfalzgraff, W. C., R. M. Hulscher, and S. P. Neshyba (2010), Scanning electron microscopy and molecular dynamics of surfaces of growing and ablating hexagonal ice crystals, *Atmos. Chem. Phys.*, *10*(6), 2927-2935, doi:10.5194/acp-10-2927-2010.

Pruppacher, H. R., and J. D. Klett (1997), *Microphysics of Clouds and Precipitation*, Kluwer Academic Publishers, Dordrecht.

Qiu, Y. Q., N. Odendahl, A. Hudait, R. Mason, A. K. Bertram, F. Paesani, P. J. DeMott, and V. Molinero (2017), Ice Nucleation Efficiency of Hydroxylated Organic Surfaces Is Controlled by Their Structural Fluctuations and Mismatch to Ice, *J. Am. Chem. Soc.*, *139*(8), 3052-3064, doi:10.1021/jacs.61312210.

Reicher, N., L. Segev, and Y. Rudich (2018), The WeIzmann Supercooled Droplets Observation on a Microarray (WISDOM) and application for ambient dust, *Atmos. Meas. Tech.*, *11*, 233-248, doi:10.5194/amt-11-233-2018.

Riechers, B., F. Wittbracht, A. Hutten, and T. Koop (2013), The homogeneous ice nucleation rate of water droplets produced in a microfluidic device and the role of temperature uncertainty, *Phys. Chem. Chem. Phys.*, *15*(16), 5873-5887, doi:10.1039/c3cp42437e.

Rogers, D. C. (1988), Development of a continuous flow thermal gradient diffusion chamber for ice nucleation studies, *Atmos. Res.*, *22*(2), 149-181, doi:10.1016/0169-8095(88)90005-1.

Rosenfeld, D., S. Sherwood, R. Wood, and L. Donner (2014), Climate effects of aerosol-cloud interactions, *Science*, *343*(6169), 379-380, doi:10.1126/science.1247490.

Roy, P., L. E. Mael, T. C. J. Hill, L. Mehndiratta, G. Peiker, M. L. House, P. J. DeMott, V. H. Grassian, and C. S. Dutcher (2021), Ice Nucleating Activity and Residual Particle Morphology of Bulk Seawater and Sea Surface Microlayer, *ACS Earth Space Chem.*, *5*(8), 1916-1928, doi:10.1021/acsearthspacechem.1c00175.

Schill, G. P., and M. A. Tolbert (2013), Heterogeneous ice nucleation on phase-separated organic-sulfate particles: effect of liquid vs. glassy coatings, *Atmos. Chem. Phys.*, *13*(9), 4681-4695, doi:10.5194/acp-13-4681-2013.

Schill, G. P., and M. A. Tolbert (2014), Heterogeneous Ice Nucleation on Simulated Sea-Spray Aerosol Using Raman Microscopy, *J. Phys. Chem. C*, *118*(50), 29234-29241, doi:10.1021/jp505379j.

Seinfeld, J. H., and S. N. Pandis (1998), *Atmospheric Chemistry and Pysics. From Air Pollution to Climate Change*, 1326

pp., John Wiley, New York.
Shardt, N., F. N. Isenrich, B. Waser, C. Marcolli, Z. A. Kanji, A. J. deMello, and U. Lohmann (2022), Homogeneous freezing of water droplets for different volumes and cooling rates, *Phys. Chem. Chem. Phys.*, *24*(46), 28213-28221, doi:10.1039/d2cp03896j.
Shaw, R. A., A. J. Durant, and Y. Mi (2005), Heterogeneous surface crystallization observed in undercooled water, *J. Phys. Chem. B*, *109*(20), 9865-9868.
Smith, R. S., and B. D. Kay (1999), The existence of supercooled liquid water at 150 K, *Nature*, *398*(6730), 788-791.
Sosso, G. C., G. A. Tribello, A. Zen, P. Pedevilla, and A. Michaelides (2016), Ice formation on kaolinite: Insights from molecular dynamics simulations, *J. Chem. Phys.*, *145*(21), 10, doi:10.1063/1.4968796.
Stan, C. A., G. F. Schneider, S. S. Shevkoplyas, M. Hashimoto, M. Ibanescu, B. J. Wiley, and G. M. Whitesides (2009), A microfluidic apparatus for the study of ice nucleation in supercooled water drops, *Lab Chip*, *9*(16), 2293-2305, doi:10.1039/b906198c.
Storelvmo, T. (2017), Aerosol Effects on Climate via Mixed-Phase and Ice Clouds, in *Annu. Rev. Earth. Planet Sci., Vol 45*, edited by R. Jeanloz and K. H. Freeman, pp. 199-222, doi:10.1146/annurev-earth-060115-012240.
Storelvmo, T., C. Hoose, and P. Eriksson (2011), Global modeling of mixed-phase clouds: The albedo and lifetime effects of aerosols, *J. Geophys. Res.*, *116*, D05207, doi:10.1029/2010jd014724.
Tamtogl, A., E. Bahn, M. Sacchi, J. D. Zhu, D. J. Ward, A. P. Jardine, S. J. Jenkins, P. Fouquet, J. Ellis, and W. Allison (2021), Motion of water monomers reveals a kinetic barrier to ice nucleation on graphene, *Nat. Commun.*, *12*(1), 8, doi:10.1038/s41467-021-23226-5.
Tarn, M. D., S. N. F. Sikora, G. C. E. Porter, J. U. Shim, and B. J. Murray (2021), Homogeneous Freezing of Water Using Microfluidics, *Micromachines*, *12*(2), 23, doi:10.3390/mi12020223.
Thürmer, K., and S. Nie (2013), Formation of hexagonal and cubic ice during low-temperature growth, *Proc. Natl. Acad. Sci. U. S. A.*, *110*(29), 11757-11762, doi:10.1073/pnas.1303001110.
Turnbull, D., and J. C. Fisher (1949), Rate of nucleation in condensed systems, *J. Chem. Phys.*, *17*(1), 71-73, doi:10.1063/1.1747055.
Twohy, C. H., and B. W. Gandrud (1998), Electron microscope analysis of residual particles from aircraft contrails, *Geophys. Res. Lett.*, *25*(9), 1359-1362, doi:10.1029/97gl03162.
Vali, G. (1971), Quantitative evaluation of experimental results on heterogeneous freezing nucleation of supercooled liquids, *J. Atmos. Sci.*, *28*(3), 402-409.
Vali, G., P. J. DeMott, O. Möhler, and T. F. Whale (2015), Technical Note: A proposal for ice nucleation terminology, *Atmos. Chem. Phys.*, *15*(18), 10263-10270, doi:10.5194/acp-15-10263-2015.
Wang, B., and D. A. Knopf (2011), Heterogeneous ice nucleation on particles composed of humic-like substances impacted by O3, *J. Geophys. Res.*, *116*, D03205, doi:10.1029/2010jd014964.
Wang, B., D. A. Knopf, S. China, B. W. Arey, T. H. Harder, M. K. Gilles, and A. Laskin (2016), Direct observation of ice nucleation events on individual atmospheric particles, *Phys. Chem. Chem. Phys.*, *18*(43), 29721-29731, doi:10.1039/C6CP05253C.
Wang, B., A. T. Lambe, P. Massoli, T. B. Onasch, P. Davidovits, D. R. Worsnop, and D. A. Knopf (2012a), The deposition ice nucleation and immersion freezing potential of

amorphous secondary organic aerosol: Pathways for ice and mixed-phase cloud formation, *J. Geophys. Res.*, *117*, D16209, doi:10.1029/2012jd018063.

Wang, B., A. Laskin, T. Roedel, M. K. Gilles, R. C. Moffet, A. V. Tivanski, and D. A. Knopf (2012b), Heterogeneous ice nucleation and water uptake by field-collected atmospheric particles below 273 K, *J. Geophys. Res.*, *117*, D00V19, doi:10.1029/2012JD017446.

Wendisch, M., P. Yang, and P. Pilewskie (2007), Effects of ice crystal habit on thermal infrared radiative properties and forcing of cirrus, *J. Geophys. Res.-Atmos.*, *112*(D8), D08201, doi:10.1029/2006jd007899.

Westbrook, C. D., and A. J. Illingworth (2013), The formation of ice in a long-lived supercooled layer cloud, *Q. J. Roy. Meteor. Soc.*, *139*(677), 2209-2221, doi:10.1002/qj.2096.

Wex, H., P. J. DeMott, Y. Tobo, S. Hartmann, M. Roesch, T. Clauss, L. Tomsche, D. Niedermeier, and F. Stratmann (2014), Kaolinite particles as ice nuclei: learning from the use of different kaolinite samples and different coatings, *Atmos. Chem. Phys.*, *14*(11), 5529-5546, doi:10.5194/acp-14-5529-2014.

Zhang, Z. Y., Y. B. Zhou, X. L. Zhu, L. F. Fei, H. T. Huang, and Y. Wang (2020), Applications of ESEM on Materials Science: Recent Updates and a Look Forward, *Small Methods*, *4*(2), 21, doi:10.1002/smtd.201900588.

Zielke, S. A., A. K. Bertram, and G. N. Patey (2016), Simulations of Ice Nucleation by Kaolinite (001) with Rigid and Flexible Surfaces, *J. Phys. Chem. B*, *120*(8), 1726-1734, doi:10.1021/acs.jpcb.5b09052.

Zimmermann, F., M. Ebert, A. Worringen, L. Schutz, and S. Weinbruch (2007), Environmental scanning electron microscopy (ESEM) as a new technique to determine the ice nucleation capability of individual atmospheric aerosol particles, *Atmos. Environ.*, *41*(37), 8219-8227, doi:10.1016/j.atmosenv.2007.06.023.

Zimmermann, F., S. Weinbruch, L. Schutz, H. Hofmann, M. Ebert, K. Kandler, and A. Worringen (2008), Ice nucleation properties of the most abundant mineral dust phases, *J. Geophys. Res.*, *113*, D23204, doi:10.1029/2008jd010655.

Zipori, A., N. Reicher, Y. Erel, D. Rosenfeld, A. Sandler, D. A. Knopf, and Y. Rudich (2018), The role of secondary ice processes in mid-latitude continental clouds, *J. Geophys. Res.*, *123*(22), 12762-12777, doi:10.1029/2018JD029146.

Zobrist, B., T. Koop, B. P. Luo, C. Marcolli, and T. Peter (2007), Heterogeneous ice nucleation rate coefficient of water droplets coated by a nonadecanol monolayer, *J. Phys. Chem. C*, *111*(5), 2149-2155, doi:10.1021/Jp066080w.

Zobrist, B., C. Marcolli, D. A. Pedernera, and T. Koop (2008), Do atmospheric aerosols form glasses?, *Atmos. Chem. Phys.*, *8*(17), 5221-5244.

Zrimsek, A. B., N. H. Chiang, M. Mattei, S. Zaleski, M. O. McAnally, C. T. Chapman, A. I. Henry, G. C. Schatz, and R. P. Van Duyne (2017), Single-Molecule Chemistry with Surface- and Tip-Enhanced Raman Spectroscopy, *Chem. Rev.*, *117*(11), 7583-7613, doi:10.1021/acs.chemrev.6b00552.